AMERICAN SOCIETY FOR MICROBIOLOGY | Molecular and Cellular Biology®

RESEARCH ARTICLE

A Knock-In Tristetraprolin (TTP) Zinc Finger Point Mutation in Mice: Comparison with Complete TTP Deficiency

Wi S. Lai,[a] Deborah J. Stumpo,[a] Lianqun Qiu,[a]* Roberta Faccio,[b] Perry J. Blackshear[a,c]

[a]Signal Transduction Laboratory, National Institute of Environmental Health Sciences, Research Triangle Park, North Carolina, USA

[b]Department of Orthopedics, Washington University School of Medicine, St. Louis, Missouri, USA

[c]Departments of Medicine and Biochemistry, Duke University Medical Center, Durham, North Carolina, USA

ABSTRACT Tristetraprolin (TTP) is a tandem CCCH zinc finger protein that can bind to AU-rich element-containing mRNAs and promote their decay. TTP knockout mice develop a severe inflammatory syndrome, largely due to excess tumor necrosis factor (TNF), whose mRNA is a direct target of TTP binding and destabilization. TTP's RNA binding activity and its ability to promote mRNA decay are lost when one of the zinc-coordinating residues of either zinc finger is mutated. To address several long-standing questions about TTP activity in intact animals, we developed a knock-in mouse with a cysteine-to-arginine mutation within the first zinc finger. Homozygous knock-in mice developed a severe inflammatory syndrome that was essentially identical to that of complete TTP deficiency, suggesting that TTP's critical anti-inflammatory role in mammalian physiology is secondary to its ability to bind RNA. In addition, there was no evidence for a "dominant-negative" effect of the mutant allele in heterozygotes, as suggested by previous experiments. Finally, mRNA decay experiments in mutant macrophages demonstrated that TTP can regulate the stability of its own mRNA, albeit to a minor extent. These studies suggest that RNA binding is an essential first step in the physiological activities of members of this protein family.

KEYWORDS AU-rich elements, RNA binding proteins, inflammation, mRNA decay, zinc finger proteins

Regulation of gene expression by control of mRNA stability is a critical focus of control and one that can be modulated by cellular RNA binding proteins (1, 2). Many proteins have been identified that can bind directly to transcripts, in some cases with sequence specificity and high affinity, leading to either protection of the mRNA from decay or promotion of degradation (2, 3) An example of the latter category is the tristetraprolin (TTP) family of CCCH tandem zinc finger (TZF) proteins. In the mouse, this family consists of four proteins with markedly different patterns of tissue-specific and developmental stage expression (4–8); however, in cell transfection studies, all four proteins seem to behave similarly in terms of regulating mRNA stability (9, 10).

The role of TTP as an mRNA-destabilizing and mRNA binding protein was first recognized after development of a TTP knockout (KO) mouse (11, 12). These animals developed a characteristic syndrome of failure to gain weight accompanied by loss of body fat, severe peripheral polyarthritis, myeloid hyperplasia, and autoimmunity. Since this syndrome resembled previous models of excess tumor necrosis factor alpha (TNF) (13, 14), we tested the hypothesis that excess TNF was involved in its development. The weekly administration of anti-TNF antibodies to KO mice shortly after birth largely prevented the development of the KO phenotype (11). In addition, TTP knockout mice interbred with mice deficient in both types of TNF receptor developed essentially none of the characteristics of the TTP KO phenotype (15). Both of these studies demonstrated

Received 13 September 2017 **Returned for modification** 2 October 2017 **Accepted** 25 November 2017

Accepted manuscript posted online 4 December 2017

Citation Lai WS, Stumpo DJ, Qiu L, Faccio R, Blackshear PJ. 2018. A knock-in tristetraprolin (TTP) zinc finger point mutation in mice: comparison with complete TTP deficiency. Mol Cell Biol 38:e00488-17. https://doi.org/10.1128/MCB.00488-17.

Address correspondence to Perry J. Blackshear, black009@niehs.nih.gov.

* Present address: Lianqun Qiu, Department of Pathology, The University of Texas Health Science Center at San Antonio, San Antonio, Texas, USA.

that a chronic effective excess of TNF was playing a major pathogenetic role in the development of the TTP deficiency phenotype.

We then showed that macrophages derived from the TTP KO mice secreted more TNF than control cells in response to lipopolysaccharide (LPS) and that this was associated with commensurate increases in TNF mRNA levels in the knockout cells (12). These increased mRNA levels were found to be largely due to stabilization of the TNF mRNA in the TTP KO macrophages (12). We ultimately found that TTP, through its TZF domain, could bind directly to the 3′ untranslated region (3′UTR) of the TNF mRNA and that this started a chain of events resulting in the deadenylation of the mRNA and its ultimate destruction (12, 16).

The ideal binding sequence for the TTP TZF domain in mRNA was UUAUUUAUU, a sequence that is repeated several times within the TNF AU-rich element (ARE); most of these 9-mers are highly conserved among mammalian TNF mRNAs (17). When synthetic peptides comprising the TTP TZF domain were used in RNA binding assays with purified components, the K_d (dissociation constant) of the TTP TZF domain peptide to the optimal mRNA 9-mer was approximately 3 nM at room temperature (18). A structure of the TZF domain from the TTP family member ZFP36L2 (Tis11d) in complex with this same 9-mer was analyzed by Wright and colleagues (19). Major protein-RNA interactions included stacking interactions between the RNA bases and aromatic rings of conserved hydrophobic amino acids within or leading into the tandem zinc finger domains, as well as electrostatic interactions. Strikingly, the RNA binding site was unstructured in this complex (19), suggesting that secondary structure of the mRNA might be deleterious to protein binding.

One important finding from the RNA binding studies was that mutation of any one of the eight cysteines and histidines within the TZF domain completely abrogated high-affinity RNA binding (20), even when the other finger remained intact. When point mutants of this type, as well as those with several other nonbinding mutations within the TZF domain, were used in cotransfection assays of TTP activity to promote the decay of TNF, granulocyte-macrophage colony-stimulating factor (GM-CSF), and interleukin-3 (IL-3) transcripts, we found severalfold-increased accumulation of the target transcripts compared to the starting levels (16, 20). These data suggested that the mutant proteins were having a deleterious effect on the target mRNA degradation machinery, possibly by interfering with protein factors involved in mRNA decay.

These findings suggested the possibility that a similar mutant form of TTP could exert a "dominant-negative" effect in intact animals. To test this idea, we have made the analogous mutation using knock-in (KI) technology in the mouse, allowing us to determine whether the mutant allele had a dominant-negative effect on the wild-type (WT) allele. These mice, and cells derived from them, also allowed us to address several other long-standing questions concerning TTP activity: (i) whether all of TTP's physiological effects stem from its initial RNA binding ability, (ii) whether TTP can regulate the stability of its own mRNA, and (iii) whether the effect of TTP to promote the decay of its target mRNAs is a transient effect that occurs only immediately after its induction or can be sustained for several hours after its initial synthesis.

RESULTS

Nature of the C116R mutation. We introduced a T-to-C substitution in exon 2 of the *Zfp36* locus, encoding TTP, in an attempt to create a mouse that would express the TTP protein with a mutated zinc-coordinating residue in one of its TZF domains, as shown in the scheme in Fig. 1A. The tandem zinc finger (TZF) domain of mouse TTP is illustrated in Fig. 1B, which shows the location of the cysteine-to-arginine (C116R) mutation in the third cysteine of the first zinc finger. This was accomplished by mutating a single T to C in the cysteine codon (Fig. 1A). Similar to results obtained with the human TTP protein with the analogous mutation (Fig. 1D, lanes 3 and 4), when this mutant protein was used in RNA gel shift analyses, the binding of the full-length mutant TTP protein to a TNF-based RNA probe was completely abrogated (lanes 5 and

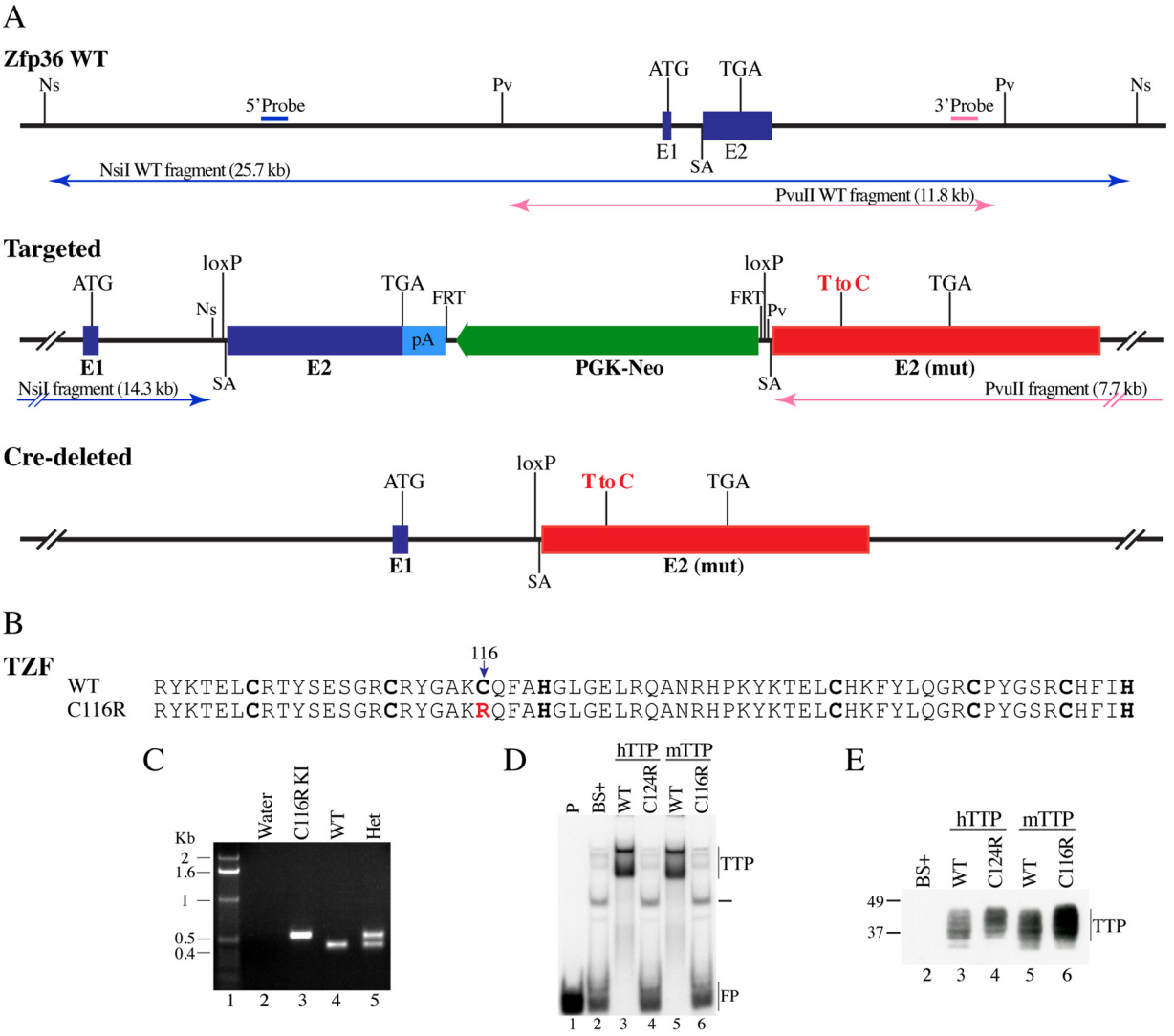

FIG 1 Scheme of *Zfp36* gene targeting and the TZF domain mutant. (A) Schematic representation of the mouse *Zfp36* locus, the targeted features in the mutant locus, and after the Cre-mediated deletion of *Zfp36* WT exon 2 and the PGK-Neo selection cassette. The arrows indicate the sizes of the NsiI- or PvuII-digested fragments from normal *Zfp36* or from the correctly targeted mutant locus. Ns, NsiI; Pv, PvuII; E1, exon 1; E2, exon 2; SA, splice acceptor; loxP, specific binding sites for Cre DNA recombinase; FRT, flippase recognition site; pA, BGH-poly(A) (in light blue). Exons from WT *Zfp36* are colored dark blue, the mutated exon 2 (with a single T-to-C substitution) is in red, and the PGK-Neo selection cassette is in green. (B) Mouse TTP TZF domain peptide sequence, with the arrow pointing at position 116 in the intact protein, where the cysteine in the WT protein has been changed to an arginine in the mutant protein (C116R) by the single T-to-C substitution in *Zfp36*. (C) Image of a PCR genotyping gel. Lane 1 shows the DNA ladder, lane 2 used water instead of a DNA template, the single 546-bp band in lane 3 demonstrates that the normal exon 2 of *Zfp36* has been deleted from both alleles, the single 446-bp band in lane 4 indicates a normal *Zfp36* locus in both alleles, and the double band in lane 5 shows that the normal exon 2 of *Zfp36* has been deleted from one allele (upper band) and the other allele remains WT (lower band). (D) Sample gel shift using a TNF mRNA-based ARE probe. In lane 1, probe alone was run on the gel; in lane 2, an extract from cells transfected with vector (BS+) was used (note the various bands that were formed from the binding of endogenous 293 cell proteins to the probe); in lanes 3 and 4, extracts were used from cells transfected with either WT human TTP (hTTP) (lane 3) or its point mutant (lane 4); in lanes 5 and 6, extracts were used from cells transfected with either WT mouse TTP (mTTP) (lane 5) or its corresponding point mutant (lane 6). The migrations of the major TTP-probe complexes (TTP), a readily visible endogenous 293 cell protein-probe complex (line), and the unbound free probe (FP) are indicated to the right of the autoradiograph. (E) Sample Western blot of 293 cell extracts. The lane numbers in panels D and E correspond to the same extracts used for the gel shift and the Western blot.

6). Expression in 293 cells of WT and mutant human and mouse proteins is documented in Fig. 1E.

For the analyses of TTP's effect on the stability of its own mRNA described below, it is important to note that the WT and mutant mRNAs should be identical except for the single T-to-C change at bp 377 in the sequence under GenBank accession no. NM_011756.4. Since the mutant gene remained in its endogenous *Zfp36* locus, all other aspects of *Zfp36* expression should be the same in these two lines of mice.

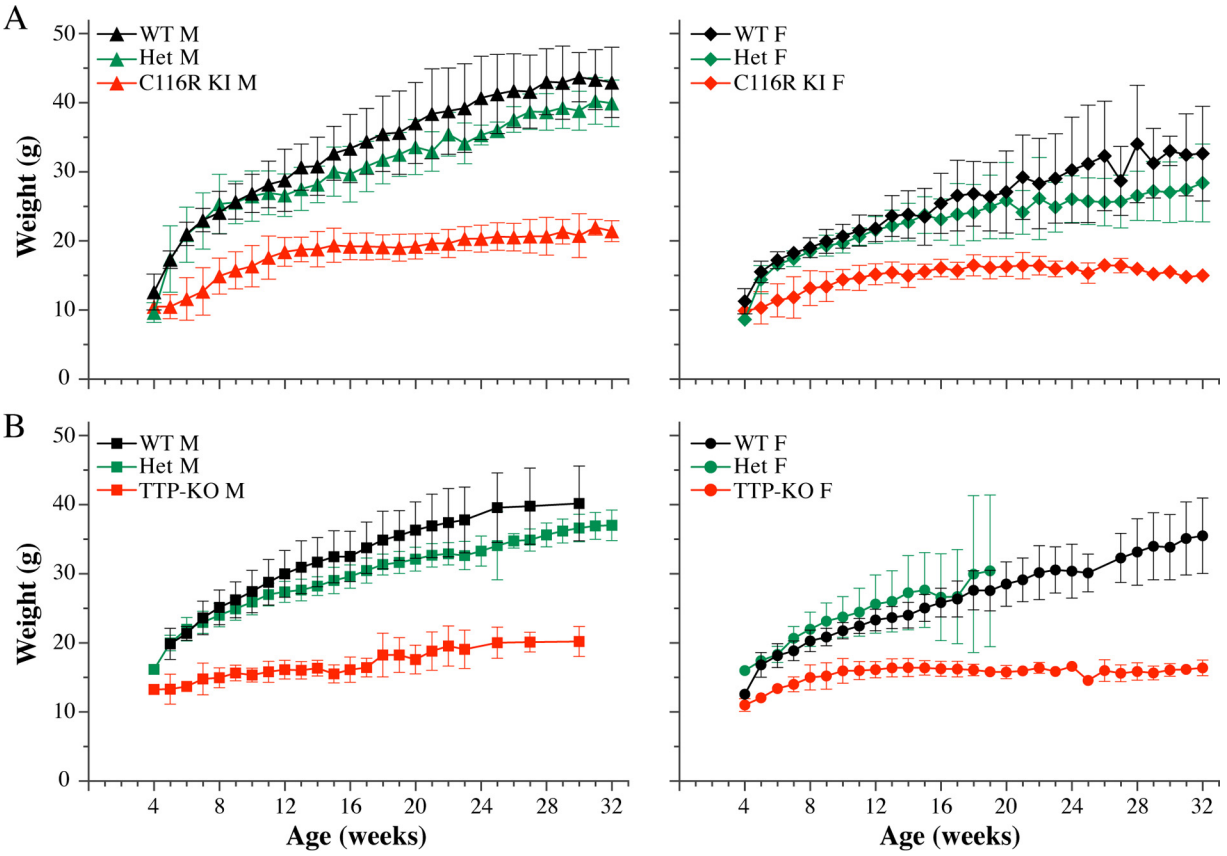

FIG 2 Growth curves of C116R KI and total TTP KO mice. Body weights were measured weekly from 4 to 32 weeks of age. The results are expressed as mean ± SD. In general, 3 to 9 mice were used in each group, although fewer mice were available in the TTP KO or C116R KI groups at older ages. (A) Average weights of homozygous C116R KI mutant mice and their corresponding WT and heterozygous (Het) counterparts; data from male mice are shown in the left panel, and data from female mice are shown in the right panel. (B) Average weights of homozygous TTP KO mice and their corresponding WT and Het counterparts, with males on the left and females on the right. There were no significant differences between the body weights of homozygous KI mice and homozygous KO mice, as determined by cubic polynomial growth curve analysis. Similarly, there were no differences between the growth curves of any of the heterozygous mice and those of their WT counterparts.

Phenotype of the C116R KI mice. (i) Body weight. The characteristic pattern of body weight gain of WT C57BL/6 mice in our colony is illustrated in Fig. 2 (left panels, males [M]; right panels, females [F]). When homozygous KI mice (Fig. 2A, red) were compared to homozygous KO mice (Fig. 2B, red), there were no statistically significant differences between growth curves for either sex. This simple measurement is a powerful index of the "TTP deficiency phenotype" in mice. This result suggests that the KI protein, despite its apparently normal regulated expression (see below), was completely ineffective at preventing the development of the KO phenotype of slow weight gain. In turn, this suggests that the actions of intact TTP to prevent development of this aspect of the TTP deficiency syndrome could be completely blocked by the single mutation that prevented binding to its target mRNAs.

The other important observation in this experiment concerned the comparison of the growth curves between the heterozygous KI animals and the heterozygous KO animals. Both the heterozygous KO and KI male mice had slightly but not significantly lower body weights than their WT controls at most ages (Fig. 2, left panels). Similarly, there were no significant differences between the two types of female heterozygotes and their WT counterparts (Fig. 2, right panels). These data indicate that there was no further deleterious effect of the KI mutation over and above its loss of function. This provides strong evidence that the mutant protein does not exert a "dominant-negative effect" on this aspect of the phenotype.

(ii) Other aspects of the phenotype. In general, the other aspects of the KI phenotype closely matched those of the original KO phenotype on this genetic

TABLE 1 Absolute neutrophil, lymphocyte, and monocyte counts and their percentages of white cell counts in peripheral blood

	Male mice			Female mice		
	Absolute count, 1,000/μl (% of WBC)[a]			Absolute count, 1,000/μl (% of WBC)		
Cell type	C116R KI	WT	*P*[b]	C116R KI	WT	*P*
Neutrophils	1.96 ± 0.92 (27 ± 10)	0.69 ± 0.32 (10 ± 3)	0.003 (0.0005)	2.46 ± 1.30 (33 ± 11)	0.62 ± 0.23 (12 ± 3)	0.003 (0.0004)
Lymphocytes	4.81 ± 1.74 (66 ± 10)	5.34 ± 1.05 (85 ± 3)	NS (0.0003)	4.59 ± 1.77 (61 ± 12)	4.51 ± 1.14 (84 ± 3)	NS (0.0004)
Monocytes	0.22 ± 0.12 (2.89 ± 1.62)	0.12 ± 0.05 (1.67 ± 1.00)	0.03 (NS)	0.28 ± 0.15 (3.44 ± 1.01)	0.06 ± 0.04 (1.22 ± 0.67)	0.002 (<0.0001)
WBC	7.22 ± 2.33	6.32 ± 1.29	NS	7.50 ± 2.31	5.42 ± 1.38	0.03

[a]Results are expressed as average ± SD. Nine mice at of each group (C116R KI or WT) were used 12 ± 1 weeks of age.
[b]*P* values were determined using unpaired, two-tailed *t* tests with Welch's correction. NS, not significant.

background. Specifically, the mice developed severe polyarthritis, particularly of joints of the paws, along with accumulation of neutrophils in the soft tissues of the paws; their body fat was severely depleted in comparison to that of their control littermates; and there was evidence of severe myeloid hyperplasia, both within the bone marrow and at extramedullary sites (data not shown). They also exhibited significant increases in circulating neutrophils (Table 1) (>2-fold in males and ~4-fold in females) and monocytes (Table 1) (~2-fold in males and >4-fold in females).

(iii) Bone mineral density and erosions in the C116R mutant mice. The effects of TTP deficiency on bone metabolism were not studied in any detail in our original description of the TTP deficiency syndrome (11). To evaluate the possibility of bone loss in the KI mice, we evaluated bone mineral density in four groups of mice ($n = 5$ in each) at approximately 12 weeks of age (Table 2). In comparison with WT male mice, KI male mice exhibited a decrease in average bone mineral density of 18% ($P = 0.0062$). For the females, KI mice exhibited an average bone mineral density decrease of 24% ($P = 0.0087$).

All C116R KI mice, both male and female, exhibited red and swollen paws, starting as early as 4 weeks of age. Bone destruction in the paws was examined by both conventional radiography and micro-computed tomography (micro-CT). As shown in the upper panels (KI) of Fig. 3, the front paws of both 3-month-old C116R KI female (Fig. 3A) and male (Fig. 3B) mice exhibited soft-tissue swelling and bone changes compared to their WT counterparts (Fig. 3A and B, lower panels [WT]). The bone changes seen in the radiographs include severe erosions and osteopenia (Fig. 3A and B, upper panels). Evaluation by micro-CT showed that the KI mouse paws had severe bone erosions (Fig. 3C and D, upper panels) compared to paws from WT mice of the same age (Fig. 3C and D, lower panels). The pathological changes were more severe at older ages (compare 4-month-old male [Fig. 3C, upper panel] 6-month-old male [Fig. 3D, upper panel]).

The same paws shown in Fig. 3D were used for hematoxylin-and-eosin (H&E) staining and tartrate-resistant acid phosphatase (TRAP) staining (Fig. 4). In the KI paw, there was evidence of severe myeloid hyperplasia (H&E, arrowheads) and inflamed synovium with leukocyte infiltration (H&E, arrows). There was also widespread TRAP staining (TRAP, arrows), indicating increased numbers of osteoclasts, compared to that in the WT paw, where there was minimal detectable TRAP staining.

Taken together, these data demonstrate that the C116R mutant form of TTP, when expressed from its normal locus in intact mice and under normal physiological regulation, does not exert any obvious effects to modify the TTP deficiency phenotype in

TABLE 2 Bone mineral density

Mice[a] (sex)	BMD, g/cm^2 (avg ± SD)[b]	*P* value, KI vs WT[c]	95% confidence interval
C116R KI (male)	0.042 ± 0.004	0.0062	0.0039–0.015
WT (male)	0.051 ± 0.002		
C116R KI (female)	0.041 ± 0.007	0.0087	0.0049–0.022
WT (female)	0.054 ± 0.004		

[a]Five 12-week-old mice were used in each group.
[b]The bone mineral density (BMD) is the bone mineral content per area of bone being measured.
[c]*P* values were determined using unpaired, two-tailed *t* tests with Welch's correction.

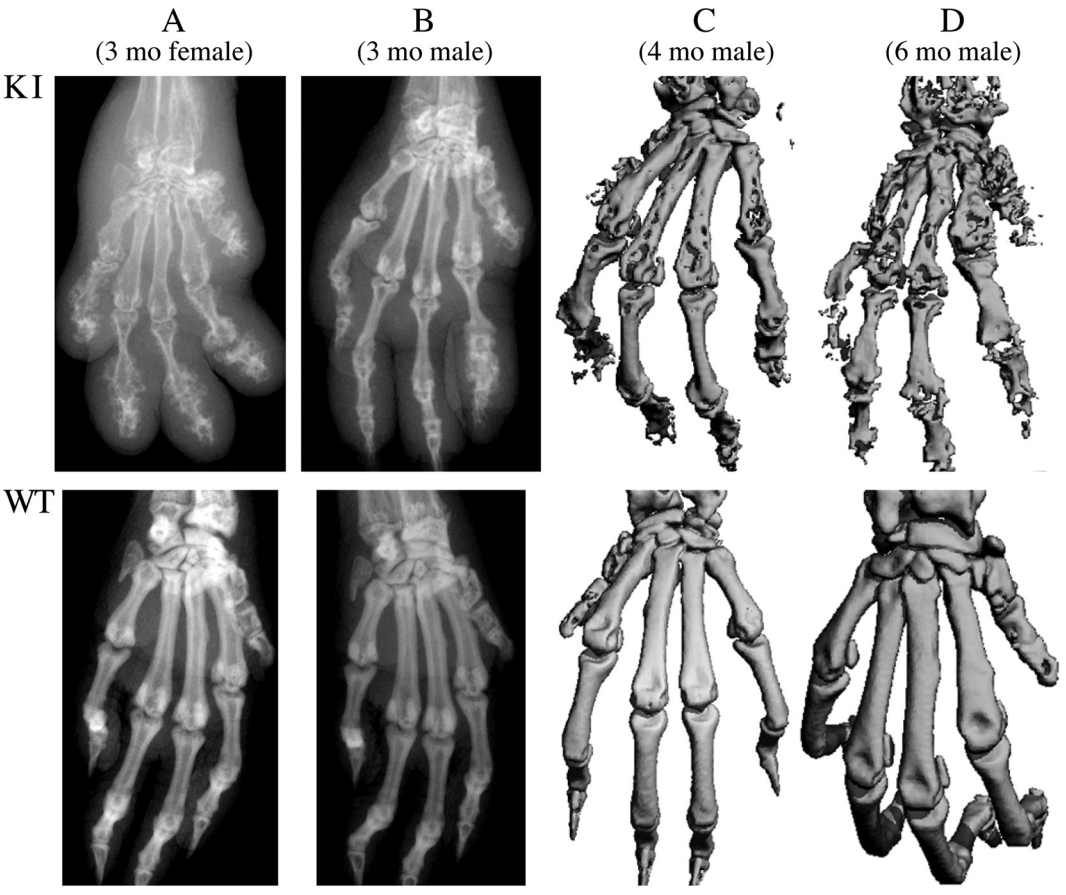

FIG 3 Paw imaging. The upper panels show the images from C116 KI mouse paws, and the lower panels show images from the WT littermates. (A and B) Mouse paw X-rays from females (A) and males (B), both at 3 months of age. (C and D) Micro-CT images of paws from 4- and 6-month-old male mice, respectively.

the mouse. This suggests in turn that the important physiological effects of TTP on mRNA stability, and its ability to function as an anti-inflammatory or "arthritis suppressor" protein, all derive from its ability to bind RNA. It is premature to conclude that TTP has no functions that cannot be attributed to its initial RNA binding, but this possibility is suggested by these results.

Responses of TTP C116R macrophages. (i) Expression of the TTP C116R mRNA and protein. With the KI approach, the manipulated gene should exhibit normal patterns of mRNA and protein expression. To test this, we evaluated bone marrow-derived macrophages (BMDM) from WT and KI mice for TTP mRNA and protein expression after LPS stimulation (Fig. 5). At the mRNA level, TTP transcripts were barely detectable at time zero in the cells of both genotypes (Fig. 5A, lanes 1 and 9), but mRNA accumulated rapidly within 15 to 30 min of LPS stimulation, reaching a peak at about 60 min (Fig. 5A, lanes 4 and 12), and then fell back to lower levels at subsequent time points. Although the initial LPS-induced expression was remarkably similar for the WT and KI cells, quantitation of the mRNA levels by Northern blotting from five similar experiments suggested that there was a modest increase in transcript levels in the KI cells at later time points after stimulation (Fig. 5B), when the TTP mRNA levels at each LPS treatment period were expressed as fractions of KI peak level.

At the protein level, there was minimal detectable protein at time zero in cells of both genotypes (Fig. 5C, lanes 1 and 6), but in both cases there was a rapid increase in immunoreactive protein that began at 30 min (not shown) and continued for 1, 3, and 6 h after LPS stimulation (Fig. 5C, lanes 2 to 4 and 7 to 9). There appeared to be a modest increase in TTP protein in the KI cells relative to the WT cells from 1 to 6 h and

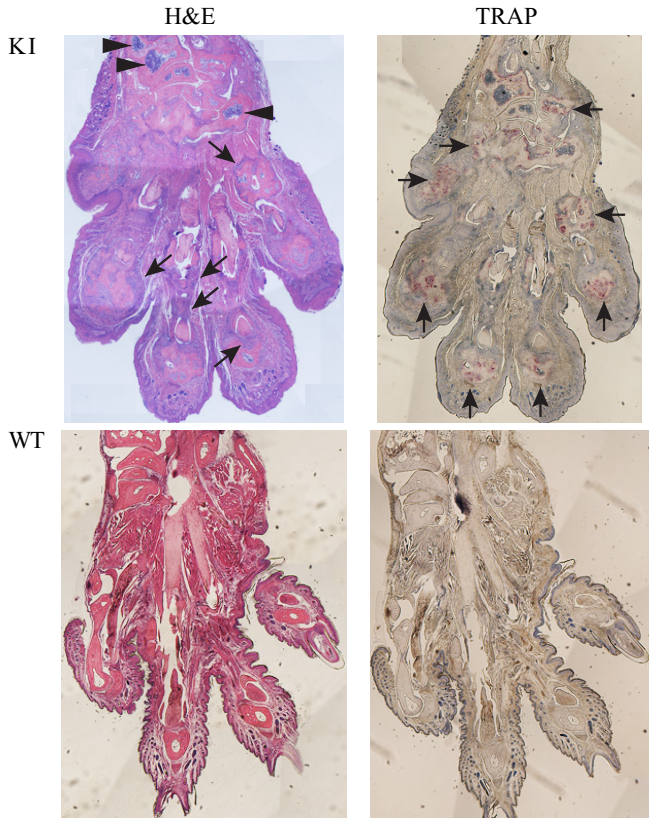

FIG 4 Paw histology. The paws shown in Fig. 3D were used for histochemical staining. The upper panels show staining from the C116 KI paw sections, and the lower panels show staining from the WT. The left panels show sections stained with H&E, whereas the right panels show sections stained for TRAP. In the H&E staining of the KI paw, the arrowheads indicate myeloid hyperplasia, and the arrows indicate synovial tissues with leukocyte infiltration. In the TRAP staining of the KI paw, the arrows point to osteoclasts, identified by their high expression of TRAP.

a more pronounced accumulation at 24 h after LPS incubation (Fig. 5C, compare lanes 5 and 10). This apparent increase in the mutant TTP protein expression may be due to the increased accumulation of the C116R mRNA in the KI cells, particularly at longer periods of LPS incubation (Fig. 5B). The characteristic SDS gel migration variants seen in this figure have been attributed to multiply phosphorylated forms of the protein (see references 21 and 22 for reviews); these appeared to be roughly similar in the WT and KI cells.

(ii) TNF mRNA accumulation and decay in TTP C116R macrophages. The best-known mRNA target of TTP is the TNF transcript, which contains numerous potential TTP binding sites within an AU-rich element in its 3′UTR, approximately 300 bases 5′ of the poly(A) tail in human and mouse. In macrophages derived from the original TTP KO mice, there was a characteristic slowing of TNF mRNA decay when tested 4 h after LPS stimulation of TTP KO macrophages, with increases in half-life of 2- to 3-fold (12). We therefore tested BMDM from WT and TTP C116R KI mice and compared their patterns of TNF mRNA accumulation after LPS stimulation (Fig. 5D and E) and their rates of mRNA decay after treatment with actinomycin D (see below). As expected, there were apparent increases in TNF mRNA levels at most time points after LPS stimulation of both the WT and KI cells (Fig. 5D). Northern blotting data from five similar experiments were quantitated by PhosphorImager analysis, and the TNF mRNA levels at each time after LPS treatment are shown in Fig. 5E, expressed as fractions of the peak level in the KI cells. There were greater accumulations of the TNF mRNA in the KI BMDM at all time points after LPS stimulation between approximately 1 and 8 h; they returned to near-normal levels after 24 h (Fig. 5E). These changes in mRNA levels were accompa-

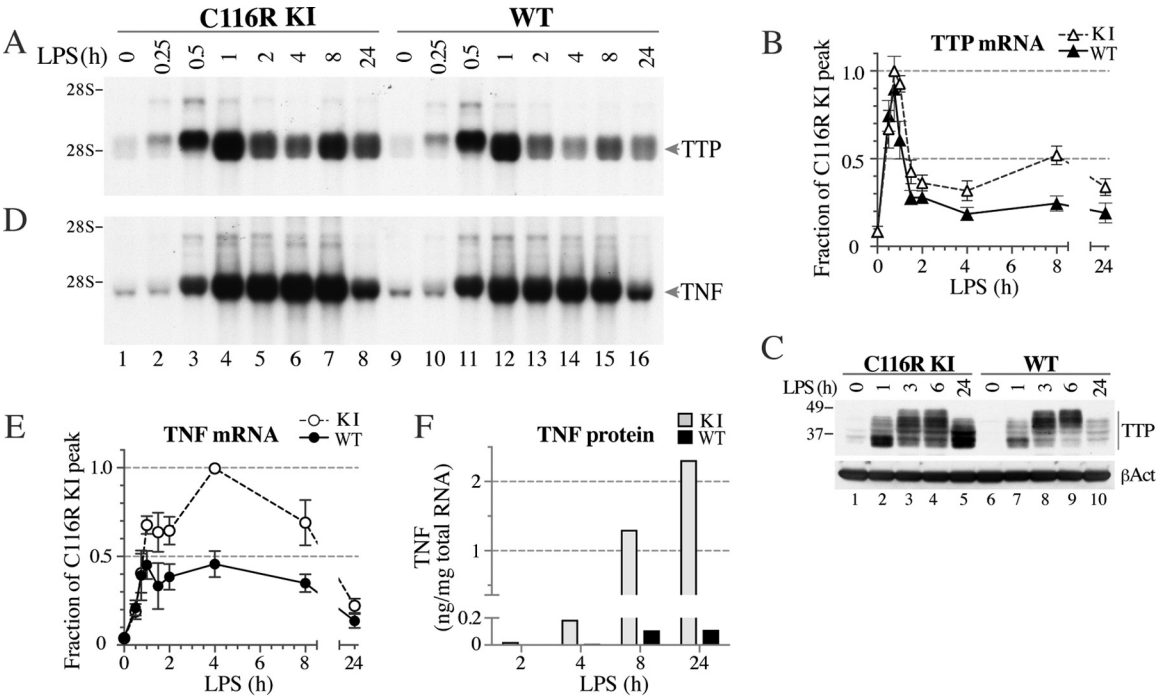

FIG 5 TTP and TNF mRNA and protein expression in BMDM after LPS stimulation. In all panels, BMDM were incubated with LPS for the times indicated. (A) Northern blot of a typical LPS treatment experiment after hybridizing to a TTP probe. Each lane was loaded with 8 μg total RNA from C116R KI (lanes 1 to 8) or WT (lanes 9 to 16) cells. (B) Relative accumulation of TTP mRNA after LPS stimulation, expressed as fractions of the peak response of the C116R KI cells (mean ± SD) from five independent experiments identical to that shown in panel A. (C) Western blot demonstrating TTP protein expression in BMDM in response to LPS. Lanes 1 to 5 contain protein extracts from C116R KI cells, and lanes 6 to 10 are from WT cells. The upper panel shows the results of immunoblotting with an anti-mouse TTP serum, and the lower panel shows the results of blotting with an antiactin antibody (Act), as indicated to the right of the blot. (D) Northern blot of an RNA sample from the experiments shown in panel A, but this time hybridized to a TNF probe. (E) Relative accumulation of TNF mRNA after LPS stimulation in the cells of the two genotypes, expressed as fractions of the peak response of the C116R KI cells (mean ± SD) from five independent experiments identical to that shown in panel D. (F) Mean values (from two independent experiments) of TNF protein released from the BMDM into the culture medium after LPS treatment for the times indicated, as measured by ELISA; the data were normalized by the amount of total RNA harvested from the cells after the LPS incubations.

nied by greatly increased amounts of TNF protein released from the KI cells into the culture supernatants (Fig. 5F).

In WT cells, TNF mRNA levels exhibit a characteristic time course after LPS stimulation, with a first peak seen approximately 1 h after stimulation, followed by a brief decline and then continued accumulation to higher levels (Fig. 5E). Because TTP protein at later LPS incubation times could be modified by multisite phosphorylation and other posttranslational events, it has been suggested that TTP is only transiently effective at promoting TNF mRNA decay after LPS induction (21). We therefore investigated the possibility that there would be different TNF mRNA decay patterns after different times of LPS stimulation. To do this, we assayed the decay of TNF mRNA in BMDM after LPS treatment of 1, 3, and 6 h. At these time points, the cells were treated with actinomycin D to stop further transcription, and then they were harvested at various times for the next 2 h. Northern blots from typical experiments of this type are shown in Fig. 6A and C. When cells were treated for only 1 h with LPS, followed by actinomycin D, there was marked stabilization of the TNF transcript in the TTP C116R KI cells (Fig. 6A). Data from five similar experiments (each with a different pair of WT and KI cells) are quantitated in Fig. 6B. The time for the TNF mRNA to decay to 50% of its original level (t_{50}) increased from 18 ± 3 min (mean ± standard deviation [SD]) in the WT cells to 69 ± 15 min in the C116R KI cells ($P = 0.0012$) under these conditions. These results are essentially identical to the effect of the TTP null mutation on macrophages (WT, 17 ± 3 min; TTP KO, 59 ± 15 min [$n = 5$, mean ± SD, $P = 0.0027$]) from a parallel study (not shown).

When the cells were stimulated with LPS for either 3 h or 6 h, the stabilization of the TNF mRNA was still readily apparent in the KI cells (Fig. 6C, lanes 2 to 8) compared to

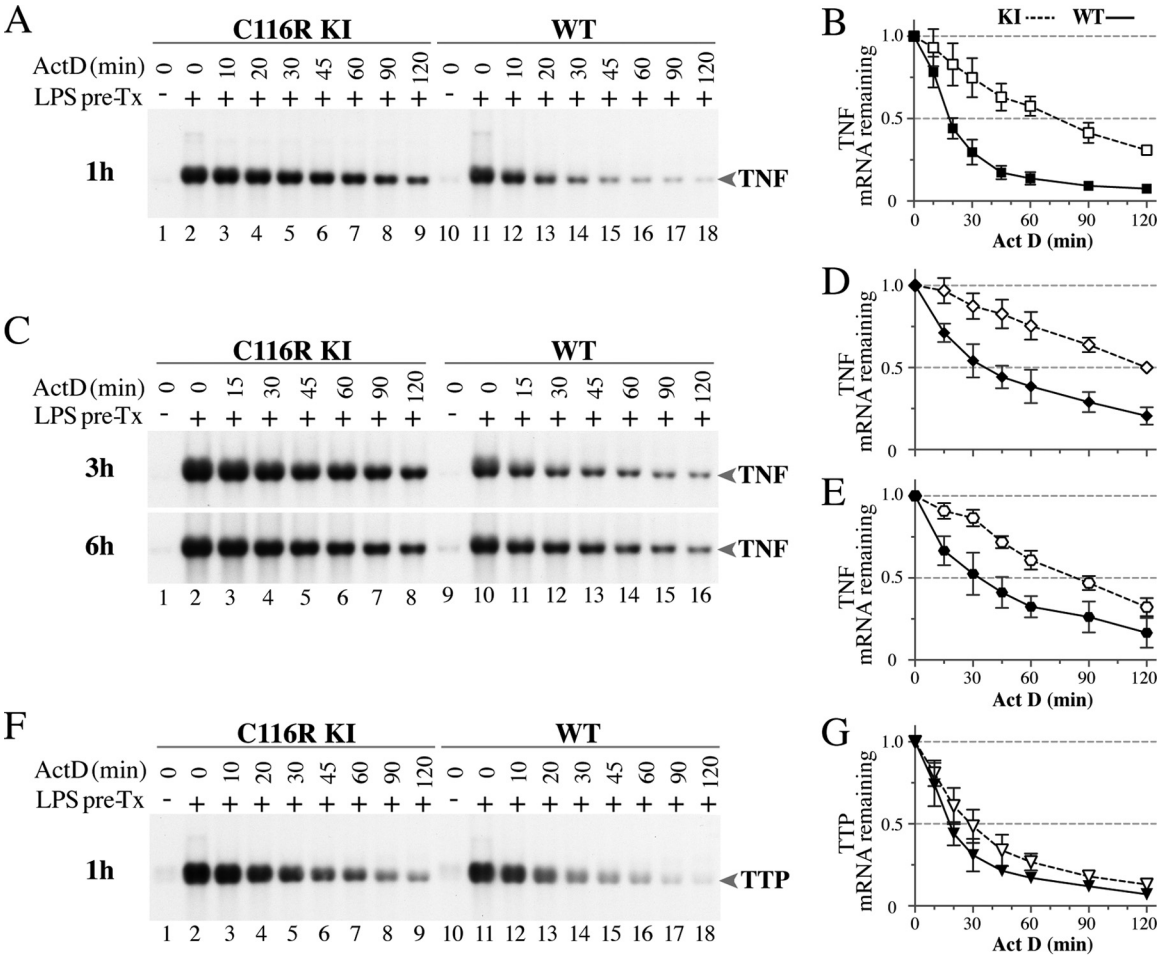

FIG 6 TNF and TTP mRNA decay in BMDM after LPS stimulation. BMDM were pretreated with LPS for 1 h, 3 h, or 6 h and then incubated with actinomycin D (Act D) for the times indicated. (A) A Northern blot hybridized to a TNF cDNA probe shows typical mRNA decay patterns from cells of each genotype treated with LPS for 1 h, followed by Act D addition and subsequent sampling. (B) Decay curves of TNF mRNA (mean ± SD) from five independent experiments identical to that shown in panel A. (C) Typical examples of Northern blots hybridized to a TNF cDNA probe after treatment of cells with LPS for 3 h (upper panel) or 6 h (lower panel), followed by the Act D incubation time courses. (D and E) Decay curves of TNF mRNA after 3 h (D) and 6 h (E) of LPS pretreatment were calculated from multiple experiments identical to those shown in panel C. Each shows means ± SD from five (D) or four (E) independent experiments. (F) Northern blot from a typical experiment with cells of both genotypes pretreated with LPS for 1 h, followed by an Act D incubation time course. The blot was hybridized to a TTP cDNA probe. (G) Combined data from five independent experiments identical to that shown in panel F (mean ± SD). See the text for half-life determinations and other details.

the WT cells (Fig. 6C, lanes 10 to 16). In cells treated with LPS for 3 h followed by actinomycin D, the TNF mRNA decay t_{50} from five similar experiments (each using a different pair of WT and KI cells) in WT cells was 38 ± 12 min (mean ± SD), and it increased in KI cells to 124 ± 13 min ($P < 0.0001$) (Fig. 6D). In cells treated with LPS for 6 h (Fig. 6E), the TNF mRNA decay t_{50} from four similar experiments (each using a different pair of WT and KI cells) increased from 33 ± 14 min (mean ± SD) in the WT cells to 81 ± 9 min in the C116R KI cells ($P = 0.0011$). These results demonstrated that the TNF mRNA was stabilized in the C116R KI cells even as long as 6 h after LPS stimulation. Thus, TTP in the WT cells was still able to promote decay of the TNF mRNA at 3 and 6 h after LPS stimulation, an observation similar to that found in the BMDM from myeloid cell TTP-deleted mice (23).

(iii) Potential autoregulation of TTP mRNA turnover. The TTP mRNA 3′UTR contains at least three potential TTP family member binding sites in a longer AU-rich region (24), and it has long been proposed that TTP can regulate the stability of its own mRNA (25, 26). We thought that using cells from the C116R KI mice would be an ideal way to test this idea, since the KI mRNA differs from the WT transcript by only a single

base, and the mutant allele is present in the native locus, where it is subjected to normal regulation. The time course data on the LPS-stimulated expression of TTP mRNA and protein shown above in Fig. 5 suggested that the mRNA levels were modestly increased in the KI cells at many time points after stimulation (Fig. 5B) and that the protein expression followed the same trend (Fig. 5C). We therefore compared TTP mRNA decay profiles by Northern blotting after 1 h of LPS treatment of WT and KI macrophages. As exemplified by a typical experiment (Fig. 6F), there was modest apparent stabilization of the TTP mRNA in the KI cells. When we averaged data from 5 identical experiments (Fig. 6G), the TTP mRNA decay t_{50} increased from 17 $\pm$ 5 min (mean $\pm$ SD) in the WT cells to 27 $\pm$ 7 min in the KI cells ($P = 0.031$). These data suggest that TTP regulates the stability of its own mRNA but that the magnitude of this change is relatively small.

(iv) NanoString analysis of other TTP target transcripts. We also performed NanoString assays using RNAs from four mRNA decay experiments after various times of LPS treatment to investigate several other potential target mRNAs that had been identified by other experiments (Fig. 7). As internal controls for the efficacy of the actinomycin D treatment, we used the very labile Dusp and Socs3 mRNAs (Fig. 7A, top panels). The levels of both control transcripts decreased rapidly to near 0% of the original after actinomycin D treatment, and their decay patterns did not differ in the WT and C116R cells (Fig. 7A). Cxcl1 and Cxcl2 mRNAs were obviously stabilized in the C116R KI cells after 1 h of LPS treatment, but the differences between cells of the two genotypes were less apparent after 3 h and disappeared altogether by 6 h (Fig. 7A). This could largely be accounted for by the almost complete lack of measurable decay of the two transcripts in cells of both genotypes after 6 h. The decay of Ier3 mRNA was moderately slowed in the C116R KI cells at all time points, differences that were significant after 3 and 6 h of LPS pretreatment, whereas the decay of the IL-10 mRNA was apparent at 1 h and 6 h but not after 3 h of LPS treatment (Fig. 7A). Cd274 mRNA decayed very little under these conditions, even though there were significant differences between the two genotypes after 1 or 3 h of LPS treatment. Ptgs2 mRNA was also relatively stable, but the decay was significantly different between the two cell types after 3 h of LPS pretreatment (Fig. 7A).

As shown above and in Fig. 7B, the TTP mRNA levels in BMDM were relatively low after the longer periods of LPS incubation. However, the slight effect of TTP on its own mRNA decay seen after 1 h (Fig. 6F) could still be detected after 3 or 6 h of LPS treatment followed by the addition of actinomycin D (Fig. 7A). The delay in TNF mRNA decay in the mutant cells noted above in Fig. 6A to E was confirmed by the NanoString assays as occurring at all three time points after LPS stimulation (Fig. 7A).

The steady-state levels of these mRNAs in the basal state and after various times of LPS stimulation are shown in Fig. 7B.

(v) Effect of cytokines and chemokines secreted by BMDM on fibroblast transcripts. As previously shown in TTP-deficient BMDM (27–29), the C116R BMDM released greater amounts of TNF protein than WT cells after stimulation by LPS (Fig. 5F). We analyzed BMDM culture supernatants collected after 24 h of stimulation with LPS from three different pairs of WT and C116R cells by multiplex analysis. In agreement with the enzyme-linked immunosorbent assay (ELISA) results from typical experiments shown in Fig. 5F, the amount of TNF protein released from the C116R cells was much greater than that from the WT cells (Fig. 8A). Levels of other proinflammatory cytokines and chemokines (IL-1β, CXCL1, and CXCL2 [Fig. 8A] and CCL3 [Fig. 8B]) were also significantly increased in medium from the KI cells. Although average levels of IL-10 were apparently increased in the supernatants from the KI cells (Fig. 8A), this increase was not significant. There were no differences in IL-6 or CCL5 levels (Fig. 8B) in the culture supernatants from C116R KI and WT cells.

Given that BMDM from the C116R mice released more proinflammatory cytokines after LPS stimulation than cells from WT mice and that fibroblasts responding to proinflammatory cytokines released from macrophages in turn produce chemokines

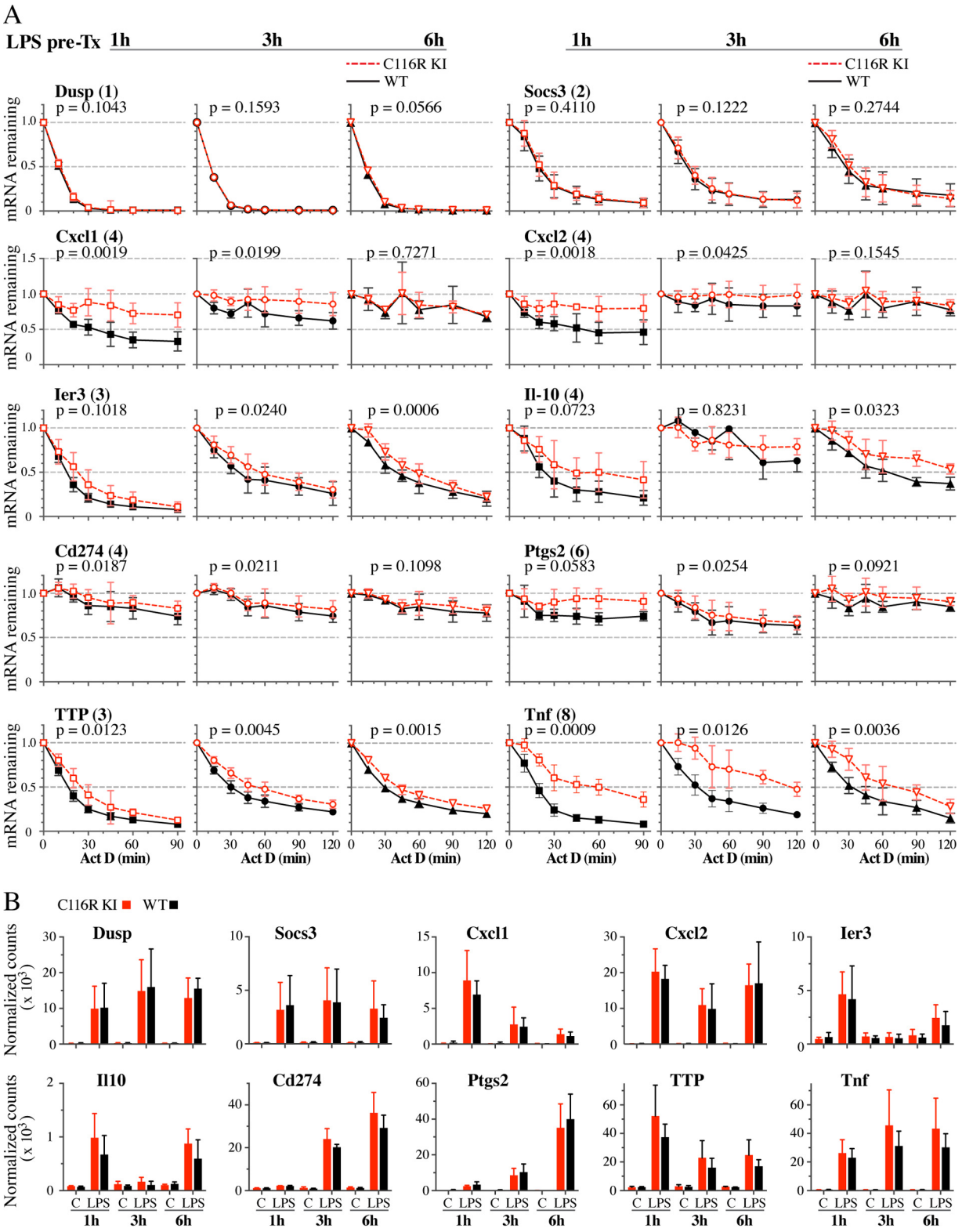

FIG 7 NanoString analysis of BMDM mRNA decay. For NanoString analyses, we used total RNA samples from decay experiments represented by the Northern blots in Fig. 6A and C, from C116R KI or WT BMDM pretreated with LPS for 1 h, 3 h, or 6 h, followed by actinomycin D time courses. (A) Data are shown as fractions of the original mRNA remaining (mean ± SD; $n = 4$) during the Act D time course, with a value of 1.0 set for the samples taken before Act D was added. The numbers in parentheses following the name of the mRNA indicate the numbers of core TTP binding sites (UAUUUAU) found in the mRNA 3′UTR. The *P* values beneath the mRNA names indicate the variation in responses between the two genotypes; see Materials and Methods for their determination. GenBank accession numbers for the transcripts are listed in Materials and Methods. (B) Data are shown for mRNA levels (normalized counts) in KI or WT cells under control conditions (C) or after incubation in LPS for the times indicated.

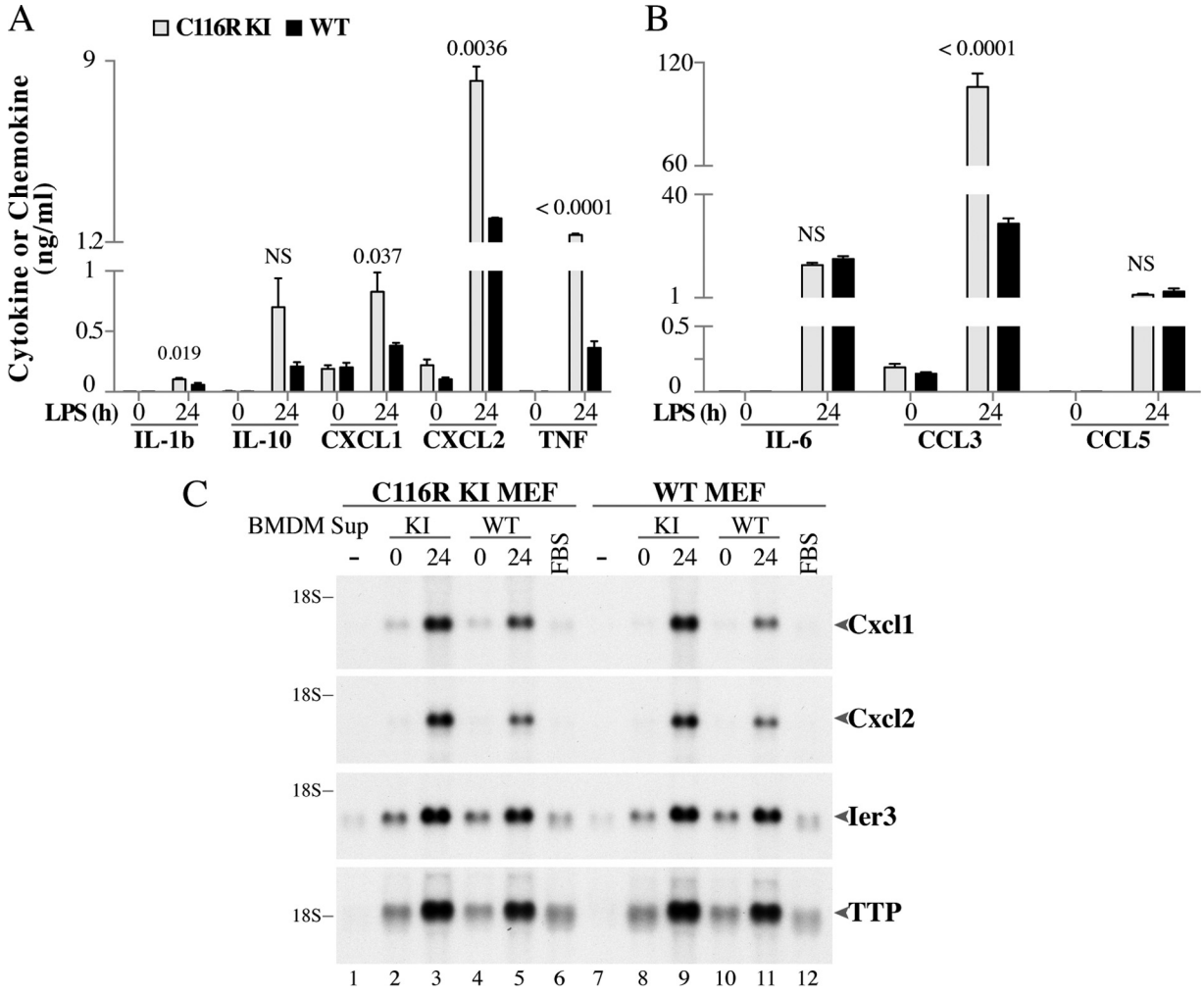

FIG 8 Cytokines and chemokines released into BMDM culture supernatants. (A and B) Levels of cytokines and chemokines released into the incubation medium (1% FBS in RPMI) of BMDM from WT or C116R KI mice after incubation for 24 h either without (0) or with (24) LPS added to the medium. The data are from three independent experiments that each consisted of a different pair of C116R KI and WT mice (mean ± SD) The numbers above the C116R KI bars indicate the *P* values from comparing the results of the KI and WT cells after 24 h of LPS incubation using unpaired two-tailed *t* tests with Welch's correction (NS, not significant). These culture supernatants were then used to treat MEFs isolated from WT and C116R embryos. (C) Representative Northern blots of RNA isolated from MEFs that were hybridized to Cxcl1, Cxcl2, Ier3, or TTP cDNA probes. The migration positions of the mRNAs are indicated to the right of the blots, and the migration position of the 18S RNA is indicated to the left. Lanes 1 to 6 were loaded with RNA from C116R KI cells, and lanes 7 to 12 contained RNA from WT cells. MEFs either remained in the serum starvation medium (lanes 1 and 7) or were changed to BMDM culture supernatants from C116R KI or WT cells (BMDM sup). These were collected from BMDM under conditions without LPS (0; lanes 2, 4, 8, and 10) or after LPS treatment for 24 h (24; lanes 3, 5, 9, and 11) or were changed to fresh 1% FBS in RPMI (FBS, lanes 6 and 12). Cells were harvested for RNA purification after 30 min of further incubation. Three similar experiments, each using a different pair of C116R and WT MEFs, were performed, and the results were similar to those shown in panel C.

that promote leukocyte recruitment (see references 30 and 31 for review), we investigated whether supernatants from these BMDM could induce heightened chemokine responses in WT and C116R mouse embryo fibroblasts (MEFs). After a 30-min incubation with culture medium from 24-h LPS-stimulated BMDM, medium from the C116R KI cells stimulated increased accumulations of Cxcl1 and Cxcl2 mRNAs in both WT and C116R KI MEFs (Fig. 8C). Ier3 and TTP mRNAs were less obviously affected (Fig. 8C).

Responses of TTP C116R MEFs. We next tested whether the responses of TTP C116R primary fibroblasts were similar to those seen previously in complete TTP KO fibroblasts (29, 32). To do this, we exposed these cells to two proinflammatory stimuli, TNF and interleukin-1β (IL-1β), and to fetal bovine serum (FBS), a potent stimulator of TTP induction in fibroblasts (16, 32) (Fig. 9A). FBS induced the expression of Ier3 and TTP mRNAs in both C116R KI and WT mouse embryo fibroblasts (MEFs) (Fig. 9A, lanes 2 and 6) but had a minimal effect on the expression of Cxcxl1 or Cxcl2 mRNA.

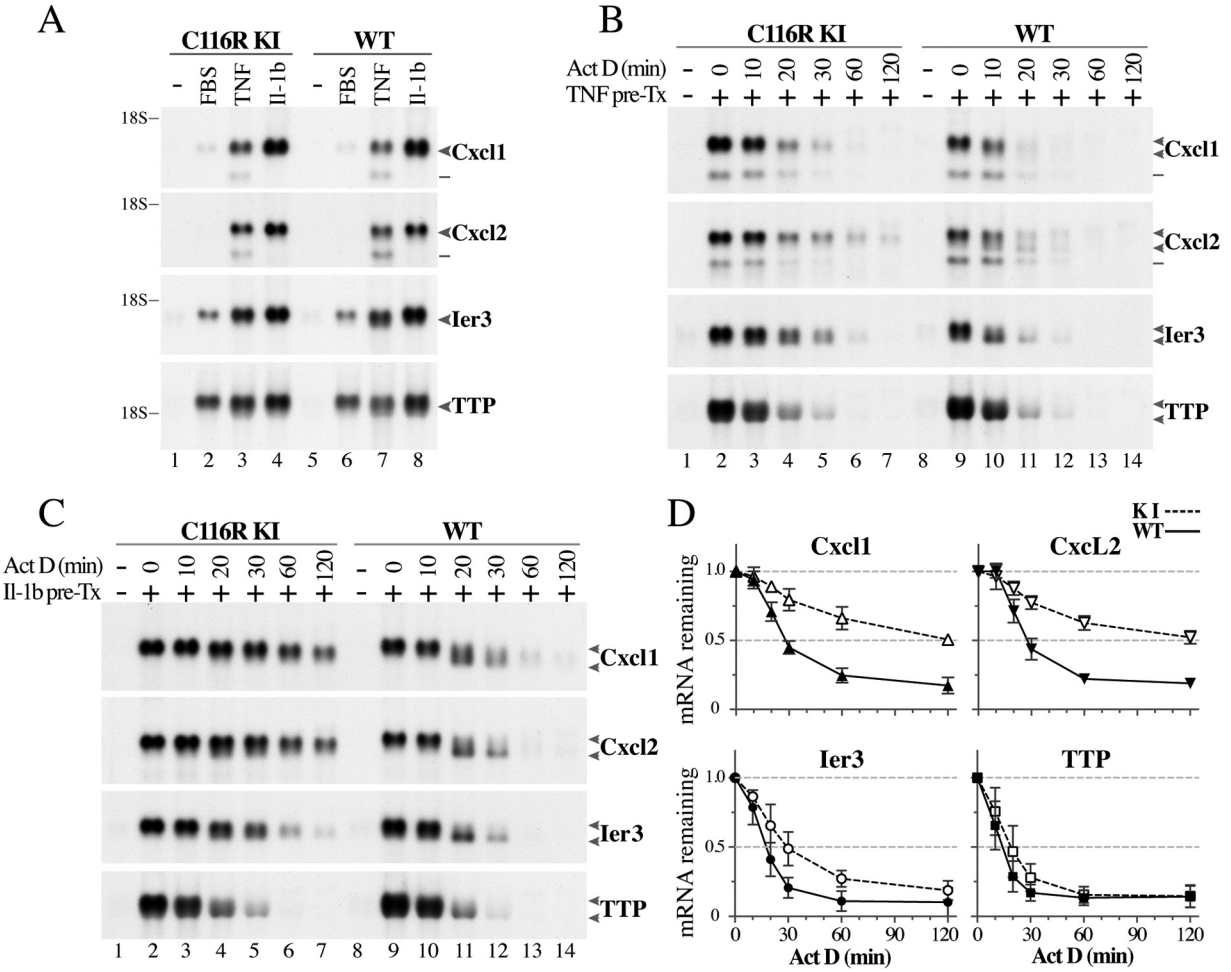

FIG 9 mRNA decay in MEF. MEFs were serum starved overnight before the indicated treatments. Each type of experiment shown is representative of three similar experiments, each using a different pair of C116R KI and WT MEF. (A) MEFs of the indicated genotype were either left untreated (lanes 1 and 5) or treated with 10% FBS (lanes 2 and 6), 10 ng/ml TNF (lanes 3 and 7), or 10 ng/ml IL-1 (lanes 4 and 8) for 30 min, as shown. Total cellular RNA from those treatments was used to prepare Northern blots, which were hybridized to Cxcl1, Cxcl2, Ier3, and TTP cDNA probes. The migration positions of the mRNAs are indicated; lines point to smaller species in the Cxcl1 and Cxcl2 hybridizations. (B and C) MEFs were pretreated with either TNF (10 ng/ml) (B) or IL-1 (10 ng/ml) (C) for 30 min and then incubated with Act D for the times indicated. Northern blots were hybridized to Cxcl1, Cxcl2, Ier3, or TTP cDNA probes. Representative Northern blots are shown (D) Decay curves after Act D incubation from three independent experiments identical to that shown in panel C (mean ± SD). In panels B and C, the migration positions of the mRNAs are indicated, with the upper arrow pointing to the fully polyadenylated mRNA and the lower arrow pointing to the deadenylated mRNA species. In the upper two panels of panels A and B, smaller degradation products were seen for Cxcl1 and Cxcl2 mRNAs after TNF treatment, but these were not seen after IL-1 stimulation (A and C). See the text for half-life determinations and other details.

TNF has been shown to be a major contributor to the systemic TTP deficiency syndrome (11, 27), and it is a key effector of leukocyte infiltration into specific tissues (28, 29, 33). In a previous study comparing TTP KO MEFs with their WT counterparts, we showed that TTP regulated the decay of several mRNAs encoding TNF-induced cytokines and chemokines (29). In the current study, TNF induced the expression of Cxcl1, Cxcl2, Ier3, and TTP mRNAs in both WT and C116R cells (Fig. 9A, lanes 3 and 7), with peaks of accumulation at approximately 30 min after TNF addition (not shown). We therefore performed actinomycin D time courses after 30 min of TNF stimulation. Cxcl1, Cxcl2, Ier3, and TTP mRNAs were all modestly stabilized in the C116R cells relative to WT cells (Fig. 9B, compare lanes 3 to 7 to lanes 10 to 14), all with decay profiles similar to those seen when the TTP KO and WT MEFs were compared (29).

Interleukin 1β (IL-1β) is another cytokine involved in local tissue leukocyte infiltration and inflammation (for reviews, see references 34 and 35). Exposure of the MEFs to IL-1β also caused increases in the expression of Cxcl1, Cxcl2, Ier3, and TTP mRNAs (Fig. 9A, lanes 4 and 8). After IL-1β stimulation, both Cxcl1 and Cxcl2 mRNA levels peaked

at 45 min, whereas Ier3 and TTP mRNAs peaked at 30 min (not shown). TTP protein expression in MEFs was readily detectable after 30 min of incubation with FBS, TNF, and IL-1β (not shown). There was a modest increase in TTP protein expression in the KI cells compared to WT cells after TNF and FBS stimulation, although this increase in the KI MEFs was not seen after IL-1β stimulation (not shown).

To compare the stabilities of Cxcl1, Cxcl2, Ier3, and TTP mRNAs in the C116R and WT MEFs in response to IL-1β, we first treated the cells with IL-1β for 30 min, followed by an actinomycin D time course. In each of the three experiments performed, we used MEFs prepared from pairs of littermate embryos from separate litters. As illustrated in the typical Northern blots shown in Fig. 9C, the mRNAs for Cxcl1, Cxcl2, and Ier3 remained relatively stable in the C116R cells, whereas in the WT cells they decayed much more rapidly (Fig. 9C, lanes 2 to 7 compared to 9 to 14). In addition, in the WT cells, the Cxcl1, Cxcl2, and Ier3 mRNAs exhibited the rapid generation of lower-molecular-weight mRNA intermediates, which first became apparent after 20 min of incubation with actinomycin D (Fig. 9C, lanes 11 to 14). This presumably reflects the accumulation of smaller deadenylated intermediates, a pattern that has been observed previously in the TTP-regulated decay of GM-CSF mRNA (36). In the present experiments, the effect of the C116R mutation was not only to stabilize the Cxcl1, Cxcl2, and Ier3 mRNAs but also to inhibit the formation of the deadenylated intermediates (Fig. 9C, compare lanes 4 to 7 to lanes 11 to 14). When data from the three experiments were quantitated (Fig. 9D), there was significant stabilization of Cxcl1, Cxcl2, and Ier3 mRNAs in the C116R cells. The calculated t_{50}s for these transcripts (mean $\pm$ SD) were as follows: Cxcl1, 26 $\pm$ 7 min in the WT MEFs versus 128 $\pm$ 11 min in the C116R MEFs ($P = 0.0092$); Cxcl2, 27 $\pm$ 5 min in the WT MEFs versus 161 $\pm$ 22 min in the C116R MEFs ($P = 0.024$); and Ier3, 16 $\pm$ 6 min in the WT cells versus 35 $\pm$ 4 min in the C116R cells ($P = 0.009$). In these experiments, there was only a minor difference in the decay of TTP mRNA, with a t_{50} of 12 $\pm$ 6 min in the WT cells versus 20 $\pm$ 4 min in the C116R cells ($P = 0.113$).

DISCUSSION

Previous RNA gel shift studies in cell extracts have shown that mutation of any of the eight zinc-coordinating residues within the TTP TZF domain can prevent high-affinity RNA binding (20; W. S. Lai and P. J. Blackshear, unpublished data). Similarly, cell transfection assays with the same mutants have shown that the mutant TTP is inactive in promoting target mRNA deadenylation and accelerating its decay (20, 37). These data suggest that all of TTP's physiological roles might require initial high-affinity binding to AU-rich element sites within the 3′UTRs of target transcripts. Answers to this question should be relevant to other members of the greater TTP protein family, defined by the presence of the canonical TZF domain, which are widely distributed among eukaryotes from plants to humans (38, 39).

This idea has been tested in the fission yeast, *Schizosaccharomyces pombe*, in which two different, analogous point mutations were made in the TZF domain of the single TTP family member expressed in that species, Zfs1. Based on the flocculation phenotype seen with Zfs1 deficiency, as well as a "molecular phenotype" of characteristic patterns of target transcript accumulation in the Zfs1-deficient strains, we concluded that knocking in TZF domain point mutations into the endogenous *zfs1* locus could phenocopy the complete deletion mutant (40). However, to our knowledge, the analogous mutation in an endogenous locus has not been attempted in a metazoan organism.

In the present studies, we made a single-base mutation in the endogenous mouse *Zfp36* locus, encoding TTP, that resulted in a C-to-R mutation at C-116 in the expressed protein (GenBank accession no. NP_035886.1). We demonstrated essentially normal regulation of the mutant TTP mRNA and protein in response to stimuli in cultured cells from WT and littermate homozygous TTP KI mice, with perhaps slightly more stable C116R mRNA and a moderate to more pronounced increase in the mutant TTP protein accumulation after longer stimulation with LPS. Based on several aspects of the phenotype, we could not distinguish the phenotype of these mutant mice from that of

the original TTP KO mice, suggesting that most if not all of TTP's roles in normal physiology stem from its initial ability to bind to AU-rich targets with high affinity. By extension, this general concept could apply to the family members found throughout eukaryotes.

However, there are several examples in the literature of other possible TTP effects, for example, effects on gene transcription (41–43). This is plausible because of TTP's nucleocytoplasmic shuttling ability (44) and suggests that its periodic nuclear localization may be relevant to this proposed transcriptional activity. TTP family members in other species have also been proposed to have transcriptional activity, such as the two proteins of this type expressed in *Arabidopsis thaliana* (45, 46). However, we have found in previous cell-free binding experiments that TTP did not bind with appreciable affinity to sequences analogous to its RNA binding sites in single- or double-stranded DNA (Lai and Blackshear, unpublished data). Nonetheless, TTP could be interacting through its TZF domain with other DNA sequences and could be acting as a coactivator or corepressor of transcription in the absence of direct DNA binding (41, 42). Interactions of TTP with other proteins also could persist despite the zinc finger mutation. Some of these interactions are known to be modified by phosphorylation (22, 47, 48), and we expect that most TTP phosphorylations would occur normally in the mutant protein. TTP is known to interact directly with other mRNA-interacting proteins or protein complexes, such as cytoplasmic poly(A) binding protein, AUF1, and the CCR4-NOT complex (49–52), all of which could occur without the need of interaction between TTP's TZF domain and its target mRNA binding sites. However, as best we can tell from our phenotyping analyses, the phenotype of the zinc finger mutant KI mice is very similar if not indistinguishable from that of the KO mice. Nonetheless, our current experiments do not entirely exclude physiological roles for TTP that are independent of RNA binding.

We also wished to use these mice, and cells derived from them, to address several other long-standing issues relating to mammalian TTP physiology. In one case, previous studies showed that at low concentrations of transfected DNA, coexpression of target mRNAs with TTP containing a single point mutation of a zinc-coordinating residue within the TZF domain completely failed to promote mRNA deadenylation and decay (16). However, at higher levels of expression, these mutant proteins actually inhibited the deadenylation and decay of cotransfected TTP target transcripts (20). A possible explanation was that the mutant protein was interfering with protein binding partners that were involved in deadenylation and decay. It raised the question of whether an analogous allele expressed in a heterozygous live animal might exert a "dominant-negative" effect on the normal protein expressed from the WT allele. The experiments presented here show no support whatsoever for this possibility, which should have been revealed by the comparisons between the *Zfp36*$^{WT/KO}$ heterozygotes and the *Zfp36*$^{WT/KI}$ heterozygotes.

Another question concerns the effects of TTP to regulate the stability of its own mRNA. As shown in this paper and elsewhere, TTP mRNA has a remarkably short half-life in macrophages and fibroblasts after LPS and TNF stimulation, of approximately 17 and 12 min, respectively, in WT cells. In genome-wide studies of both stimulated and normally growing cells, it regularly appears within the group of mRNAs with the shortest half-lives in various types of cells. It also contains several optimal and conserved TTP binding sites within its 3′UTR, contained within a longer stretch of AU richness that has been shown to confer instability on this mRNA (53). It was certainly plausible that TTP should regulate the stability of its own mRNA, and this concept has been supported by previous cell transfection experiments (25, 26). However, we viewed the current mouse model, in which only a single base has been altered in the endogenous mRNA, as the best possible model to test this idea in various cell types.

The results of these experiments seem clear. When actinomycin D was added to macrophages analyzed 1 h after LPS stimulation, when TTP transcript levels are near their peak, and transcript decay was monitored, there was a consistent and statistically significant slowing of TTP mRNA decay. In this situation, as determined by Northern

blotting of RNA from five littermate mice in each group, the half-lives of the transcripts increased from 17 min in the WT cells to 27 min in the KI cells. In fibroblasts, there was a similar minor degree of slowing of mRNA decay in the mutant cells. The transcripts could well behave differently in different cell types or in response to different stimuli, but in this case the clear result seems to be that TTP mRNA is slightly but significantly stabilized in the absence of the functional TTP protein.

Several other aspects of this mouse model deserve mention. In the present experiments, both the heterozygous *Zfp36*$^{WT/KO}$ and *Zfp36*$^{WT/KI}$ mice exhibited slightly (although not significantly) lower body weight than their WT counterparts, suggesting that a single functional allele, even under normal physiological regulation, is not quite sufficient to maintain completely normal patterns of weight gain. Larger numbers of mice in each group would be required to document this proposed "haploinsufficiency." At the molecular level, we have found no differences in TNF mRNA decay patterns in BMDM derived from WT or *Zfp36*$^{WT/KI}$ mice (not shown). Both groups of heterozygous mice were otherwise generally healthy, although occasional mice have developed what appears to be typical "TTP deficiency syndrome" late in life. It will be interesting to dissect this possible TTP inadequacy by doing, for example, stimulation experiments with LPS or infectious diseases in intact mice.

Another interesting aspect of this study concerns the severity of the bone phenotype in the homozygous KI mice. In the original description of the phenotype of the KO mice, we described destruction of bone around the sites of the inflammatory arthritis. However, the X-ray, micro-CT, and bone mineral density results presented here suggest that there is widespread general as well as focal bone loss, not only in the joints but in the long bones of the digits and elsewhere. Within the bones of the paws, there were clear increases in stainable osteoclasts, suggesting that both the local erosions and bone loss, and perhaps the systemic osteopenia, were the result of increased osteoclast activity. The mechanisms of these effects on bone are not clear, although the proinflammatory cytokines TNF, IL-1, and IL-6 are all known to affect osteoclastogenesis (for reviews, see references 35, 54, and 55). In addition, we have found that both TNF and IL-1 induced higher levels of release of the CCL3 chemokine from the C116R KI macrophages than from WT cells (not shown). Previous studies have shown that the severity of synovial infiltration and bone erosion in the TTP KO mice could be reduced when *Ccl3* was also deleted (56), though the deletion of *Ccl3* did not appear to prevent other signs of inflammation in the TTP KO mice.

Finally, there has been some discussion in the literature that TTP is mainly or only active shortly upon its induction and that the widespread phosphorylation of the protein that occurs after translation inhibits its activity, perhaps by the sequestering of phosphorylated TTP by 14-3-3 proteins (for a review, see reference 22). In the current study, we evaluated the effects of the TTP mutant on target transcript stability at 1, 3, and 6 h after LPS stimulation of macrophages. Although there were differences in the effects of TTP deficiency on decay rates at different times among the different target transcripts, some of the targets, for example, the TNF mRNA, were clearly stabilized in the absence of functional TTP at 1, 3, and 6 h after LPS stimulation. Other differences, such as the loss of effect on Cxcl1 and Cxcl2 mRNAs after 3 h of stimulation, can probably be attributed to the nature of the mRNA time courses of these transcripts after stimulation of the cells. It seems clear from these data that TTP is active enough to promote mRNA decay at 1, 3, and 6 h after LPS stimulation in macrophages. Whether it is optimally active at these later time points cannot be determined by the present experiments.

In summary, we have developed a new point mutant model of effective TTP deficiency that has been used to answer several long-standing questions about TTP biology in the intact animal. We believe that the lessons learned from this model should be applicable to the physiological roles of the TTP family members found throughout eukaryotes. As usual, these experiments leave many questions to be addressed by future studies.

MATERIALS AND METHODS

Animal procedures, genotyping, and sequence analysis of the KI allele. Conditional knock-in (KI) mice containing a point mutation in the first zinc finger in the second exon of *Zfp36* were generated by Ozgene Pty Ltd. (Perth, Australia), using standard embryonic stem (ES) cell targeting techniques. The third cysteine in the first zinc finger was mutated to arginine by changing the first nucleotide of the codon from T to C (TGC mutated to CGC [T377C] in the sequence under GenBank accession no. NM_011756.4). The targeting construct was generated from C57BL/6 genomic DNA and cloned into the Ozgene PacF vector. The final targeting vector contained a 5′ homology arm with a *loxP* site before the wild-type (WT) exon 2 encompassing the zinc fingers and a bovine growth hormone poly(A), a phosphoglucokinase (PGK)-neomycin (Neo) cassette flanked by Flp recombinase recognition (Frt) sites, and a *loxP* site followed by a 3′ homology arm containing the mutated (T377C point mutation) exon 2. All fragments in the targeting vector were generated by PCR and confirmed by restriction enzyme digestion and sequencing. C57BL/6 ES cells were electroporated with PmeI-linearized targeting vector. Correctly targeted ES cells were identified by Southern analysis using a 5′ probe with an NsiI digestion and a 3′ probe with a PvuII digestion (Fig. 1A). The sizes of the arrows in Fig. 1A indicate the sizes of the NsiI- or PvuII-digested fragments from the normal *Zfp36* locus or from the correctly targeted mutant locus. Both probes lay outside the targeting vector. Random integrations were identified with a Neo probe and XbaI, NsiI, or EcoRI digestion. An endogenous probe was used with EcoRV digestion to detect either Cre-mediated or enhanced Flp (Flpe)-mediated deletion of the PGK-neomycin cassette. These mice permit the conditional KI of the point mutation. The targeted mice were bred with an Flpe deleter mouse to remove the PGK-neomycin cassette, resulting in mice containing a floxed wild-type exon 2 and a mutant exon 2. A conditional KI of the mutant exon 2 could be achieved by breeding with a specific Cre-expressing mouse. For our study, the targeted mice were bred with a Cre deleter mouse at Ozgene, which removed both the wild-type exon 2 and the PGK-neomycin cassette, resulting in the KI of the mutant exon 2.

Heterozygous KI mice were bred with Taconic C57BL/6N mice to remove the Cre transgene and then intercrossed to generate homozygous KI mice for the exon 2 point mutation. Offspring were routinely genotyped using a 5′ primer, 5′-AGGTTCTCCCTGGAGTTTGTGTG-3′, and a 3′ primer, 5′-GCTTTCTGAGTA GGTCCGACAG-3′. These primers amplified a 446-bp endogenous *Zfp36* WT allele and a 546-bp Cre-mediated *Zfp36* KI allele containing the point mutation in exon 2 (Fig. 1C). PCR conditions were as follows: 93°C for 2 min and then 30 cycles of 93°C for 30 s, 58°C for 30 s, and 72°C for 1 min, with a final extension at 72°C for 10 min. Confirmation of the point mutation in the KI mice was done by sequencing a 539-bp fragment of exon 2 amplified using a 5′ primer, 5′-GGGCCGAAGCTGTGGCTGGGT-3′ and a 3′ primer, 5′-TTCGAGTCACAGGGGTCCCAG-3′.

All animal procedures were conducted according to U.S. Public Health Service policy on the humane care and use of laboratory animals, and the National Institute of Environmental Health Sciences Institutional Animal Care and Use Committee approved all animal procedures used in this study.

Body weights were measured weekly from 4 weeks after birth until 32 weeks of age. We compared possible differences among the growth curves using cubic polynomial growth curve analysis (57, 58).

Histopathology and clinical pathology. Animals were euthanized between 6 and 16 weeks of age, and tissues were fixed in 10% neutral buffered formalin and used for paraffin embedding, sectioning (5-μm sections), and staining with hematoxylin and eosin. Peripheral blood was collected via retro-orbital bleeding into EDTA-containing Microvette collection tubes (Sarstedt, Inc., Newton, NC) and analyzed using a Hemavet 1700 hematology analyzer (Drew Scientific, Inc., Miami Lakes, FL). White blood cell (WBC) differential counts were also performed manually to confirm the values. For some mice, peripheral blood was collected into Microvette collection tubes containing serum gel/clotting activator (Sarstedt, Inc., Newton, NC). After clotting, the tubes were centrifuged for 5 min at 10,000 $\times$ *g* at room temperature. The resulting serum was stored at −80°C until analyzed by ELISA.

Bone mineral density determination, X-rays, and micro-CT. Four groups (n = 5 in each) of 12-week-old male and female mice, WT or C116R KI, were used for the measurement of bone mineral density and for routine radiograms. Each mouse was anesthetized with 2% isoflurane in 700 ml O_2/min (induced in a chamber at 5% isoflurane and maintained by a face mask), and whole-body (head excluded) bone mineral density was obtained using a PIXImus small-animal densitometer (Lunar, Madison, WI). Bone mineral density (g/cm^2) was expressed as bone mineral content/surface area of bone being measured. The anesthetized mice were then subjected to X-ray imaging in an MX20 system (Faxitron, Tucson, AZ).

Front paws from male WT and KI mice (age 4 and 6 months) were stabilized in 2% agarose gel and analyzed by a micro-computed tomography system (μCT 40; Scanco Medical AG, Zurich, Switzerland) to obtain three-dimensional (3D) images (59, 60).

Histology and histomorphometry. For histology to detect osteoclasts and immune infiltrates, intact front paws were fixed in 10% (vol/vol) buffered formalin overnight and decalcified by using 14% (wt/vol) EDTA in double-distilled water (ddH_2O) (pH 7.0) for 10 days, with gentle rocking and daily replacement of the solution (60). Decalcified bones were then dehydrated in graded alcohol, cleared through xylene, and embedded in paraffin. Paraffin blocks were sectioned longitudinally. Five-micrometer sections were then stained with TRAP (Sigma) to detect osteoclasts and counterstained with hematoxylin. Hematoxylin-and-eosin staining was used to evaluate the extent of inflammation.

TTP protein expression and RNA mobility shift assays. Expression constructs CMV.hTTP.tag and CMV.mTTP.tag and their zinc finger mutants for human (GenBank accession no. NP_003398.1) and mouse (GenBank accession no. NP_035886.1) TTP have been described previously (16). These plasmids were expressed in HEK293 cells using the calcium phosphate precipitation method as described previously (20,

61). Briefly, to each 10-cm plate of cells was added 0.2 μg CMV.TTP.tag or mutant DNA and 4.8 μg vector (BS+) DNA. Vector (BS+) DNA (5 μg) was added to each control plate. Cytosolic extracts were prepared 24 h after removal of the transfection mixture as described previously (37, 61). These were in final concentrations of 10 mM HEPES (pH 7.6), 40 mM KCl, 1 μg/ml pepstatin A, 0.1 mM phenylmethylsulfonyl fluoride (PMSF), 1 μg/ml leupeptin, and 20% glycerol and were stored at −80°C. Gel shift assays were performed using as a probe a [^{32}P]pCp-3′-end-labeled synthetic RNA oligonucleotide, TARE5 (based on the AU-rich element within the mouse TNF mRNA 3′UTR, GenBank accession no. NM_013693.2, bp 1301 to 1332) and the HEK293 cell extracts as described previously (61). Each probe-protein binding reaction mixture of 0.2 nM TARE5 probe and 10 μg extract protein was incubated at 20°C for 30 min in 10 mM HEPES (pH 7.6), 3 mM $MgCl_2$, 40 mM KCl, and 5% glycerol in a final volume of 50 μl. The RNA-protein complexes formed were resolved on 8% nondenaturing acrylamide (37.5:1) gels.

Macrophage cultures. Bone marrow-derived macrophages (BMDM) were obtained by culturing bone marrow cells from femurs in macrophage growth medium (RPMI 1640 medium with 10% FBS, 30% L929 cell culture supernatant, 100 U/ml penicillin, 100 μg/ml streptomycin, and 6 mM L-glutamine) in 10-cm tissue culture plates. Four or 5 days after initiating the cultures, the cells still in suspension were collected and seeded onto new plates for use in experiments. The transferred cells were fed every other day by adding 2 to 3 ml of fresh macrophage growth medium to each plate. After 7 to 10 days of culture in macrophage growth medium, the 70 to 80% confluent BMDM monolayers were incubated in RPMI 1640 medium (10 ml in each plate) supplemented with 1% FBS and the antibiotics for 16 to 24 h before the experiments.

BMDM cell culture supernatants harvested for use as agonists in primary mouse embryonic fibroblast (MEF) experiments were prepared as follows. BMDM grown to 90% confluence were incubated in 1% FBS–RPMI overnight, followed by an additional 24 h of incubation with or without 1 μg/ml LPS. The culture supernatants were collected through a filter to remove any floating cells and stored at −20°C.

Primary embryonic fibroblast cultures. Primary embryonic fibroblasts (MEFs) were prepared from embryos at embryonic day 14.5 (E14.5) of gestation. Only the bodies (heads and internal organs excluded) were used for the preparation. The genotypes of each embryo were determined using genomic DNA from the embryo head and the pair of PCR primers describe above. MEFs were cultured in 10-cm plates in Dulbecco modified Eagle medium (DMEM) with 10% FBS, 100 U/ml penicillin, 100 μg/ml streptomycin, and 2 mM L-glutamine. Four pairs of MEF cultures from littermate mice (C116R KI and WT), each pair from a different litter, were used in experiments at passages 3 to 8. When MEFs in culture reached 80 to 90% confluence, the cell monolayers were rinsed with DMEM and incubated in serum starvation medium (DMEM with 0.5% FBS, 100 U/ml penicillin, and 100 μg/ml streptomycin) for 16 to 24 h before the experiments.

Cell treatments, RNA preparation, and Northern blotting. For each time course experiment using BMDM or MEFs, as indicated, 4 plates of cells from each genotype were set aside as controls (untreated), and 3 plates of cells were used for each time point stimulation with the indicated reagent (LPS [Sigma L6529], recombinant mouse TNF [R&D Systems], and recombinant mouse IL-1 [R&D Systems]). As stock solutions, LPS was reconstituted in H_2O to 1 μg/μl, and TNF and IL-1 were reconstituted to 10 ng/μl in phosphate-buffered saline (PBS) with 0.2% bovine serum albumin (BSA). At the end of each treatment period, cell monolayers were quickly rinsed in cold PBS and lysed in lysis solution (Illustra RNAspin mini; GE Healthcare). The lysates from the 3 plates from the same treatment time point (or 4 untreated plates) were pooled, and cellular RNA was prepared according to the manufacturer's protocol.

The mRNA decay assays were performed as follows. For each experiment, 4 plates of cells of each genotype were used as controls (untreated), and 4 plates were used as pretreatment references (i.e., after stimulation with LPS in the case of BMDM or with TNF or IL-1 in the case of MEFs). At the end of the indicated pretreatment period, these reference plates were quickly rinsed with cold PBS, and the cells in monolayers were lysed in lysis solution. Thereafter, three plates of cells were combined for use for each mRNA decay point. Actinomycin D (Sigma, A4262; 5 μg/ml) was added to these plates precisely at the end of the indicated pretreatment period to stop RNA transcription, and the cells were further incubated for the indicated times, followed by cold PBS rinses and cell lysis as described above.

For Northern blotting, each gel lane was loaded with 8 μg of total RNA unless otherwise indicated. Northern blotting was performed, and the α-^{32}P-labeled probes for mouse TNF, TTP, Ier3, and Cxcl1 mRNAs were prepared, as described previously (4, 9, 32). The probe for mouse Cxcl2 mRNA was prepared from a Cxcl2 3′UTR cDNA amplified using RNA from Raw264.7 cells stimulated with LPS and a pair of PCR primers (5′ primer 5′-CTGGATCGTACCTGATGTGCCTC-3′ and 3′ primer 5-AACAGACGTTTTTATTTTTTGTTATTTGTAAAAATACATG-3′, bp 431 to 453 and 1044 to 1083 of the sequence under GenBank accession no. NM_009140.2, respectively). The blots were quantitated using a PhosphorImager, and the probe-bound mRNA volumes were obtained using Volume Quantification (ImageQuant; Molecular Dynamics).

NanoString RNA analysis. Total cellular RNA from BMDM used in the RNA decay assays was analyzed using the NanoString nCounter method (62) for a specific group of mRNAs. As is customary for this technique, the observed counts were normalized by a series of internal spike-in controls and also for a set of housekeeping controls that had been previously validated as stable during LPS actinomycin D treatment, which represented a range of expression levels that spanned the expected experimental counts. GenBank accession numbers for the transcripts presented in Fig. 7 are as follows: Cxcl1, NM_008176.1; Cxcl2, NM_009140.2; Ier3, NM_133662.2; IL-10, NM_010548.1; Dusp, NM_010090.2; Socs3, NM_007707.2; Cd274, NM_021893.3; Ptgs2, NM_011198.4; Zfp36 (TTP), NM_011756.3; and TNF, NM_013693.2.

Antibodies and Western blotting. At the end of the indicated reagent treatment periods, cultured cell monolayers were scraped into ice-cold PBS and centrifuged at 600 × *g* at 4°C for 5 min. The cell pellets were rinsed quickly with ice-cold water containing 0.2 mM PMSF and 1 μg/ml pepstatin A and

then lysed on ice for 10 min in lysis buffer (50 mM Tris-HCl [pH 8.3], 150 mM NaCl, 1% NP-40, 5 mM EDTA, 5% glycerol, 2 mM dithiothreitol [DTT], 0.8 μg/ml leupeptin, 0.2 mM PMSF, and 1 μg/ml pepstatin A). Lysates were centrifuged at 4°C for 15 min at 14,000 $\times$ *g*. The supernatants were stored at −80°C with glycerol added to 20% (vol/vol). Equal amounts of protein (100 μg/lane, or as indicated) were resolved on 12% SDS-polyacrylamide gels and then transferred onto nitrocellulose membranes (GE Healthcare). The membranes were preincubated in Tris-buffered saline with 0.5% Tween 20 (TBS-T) with 5% dry milk for 1 h, followed by incubation with an antiserum against mouse TTP (63) at a 1:10,000 dilution in TBS-T–5% dry milk at 4°C overnight. Blots were rinsed with TBS-T and incubated with a secondary antibody conjugated to horseradish peroxidase (Bio-Rad) for 60 min at room temperature. After rinsing with TBS-T, the blots were developed using enhanced chemiluminescence (ECL) (Thermo Scientific). The blots were then stripped (Western blot stripping buffer; Thermo Scientific) and reprobed with an antiactin antibody (Abcam) at a 1:50,000 dilution.

ELISA, cytokine/chemokine multiplex assay, and hematology. After the indicated LPS incubation period, supernatants were collected from the BMDM cell cultures and centrifuged briefly to remove floating cells. Secreted TNF was determined by ELISA as described previously (28). The TNF protein readout was corrected by the total volume of supernatant collected, as well as by the total RNA yield from the indicated sample (i.e., TNF [pg/ml] $\times$ supernatant [ml]/total RNA [μg]).

Supernatants of BMDM cell cultures used as agonists in MEF experiments were analyzed with a mouse cytokine/chemokine magnetic bead panel (Milliplex MAP; EMD Millipore) on a Luminex-200 instrument.

Statistical analysis. Data are presented as means $\pm$ SD. In the RNA decay experiments, the value obtained after a period of stimulation (i.e., pretreatment references) was set at 1, with data from the actinomycin D treatment time course expressed as a fraction of that original value. In some cases, the time to decay (t_{50}) of an assayed mRNA was defined as the time at which the mRNA decreased to its 50% level during the actinomycin D treatment time course, as analyzed by interpolation using nonlinear regression (i.e., finding an *X* value [actinomycin D min] for *Y* at 0.5) (Prism 6; GraphPad). The differences in t_{50} between the KI and the WT groups were compared (Prism 6; GraphPad) by two-tailed unpaired Student *t* tests (with Welch's correction) from 5 individual experiments (unless otherwise indicated); the difference between the two groups was considered significant when the test *P* value was <0.05. In analysis of the NanoString assay results, the 2-way analysis of variance (ANOVA) with Sidak's multiple-comparison test was used to determine how an mRNA decay response was affected by two factors: (i) the two different genotypes and (ii) the treatment with LPS followed by an actinomycin D time course. The difference in responses of the two genotypes was considered significant when the test *P* value was <0.05.

ACKNOWLEDGMENTS

We are grateful to Michael Fessler and Robert Oakley for constructive comments on the manuscript and to Grace Kissling and Min Shi for help with the statistical analyses. We thank the Comparative Medicine Branch, NIEHS, for rodent care and animal imaging and Sukhdev Brar and Debra H. King of the Cellular and Molecular Pathology Branch, NIEHS, for cytokine assays and blood counts.

This research was supported by the Intramural Research Program of the National Institute of Environmental Health Sciences (NIH), by NIH grants R01 AR053628 and AR066551, and by Shriners Hospital grant 85100, all to R.F.

REFERENCES

1. Fukao A, Fujiwara T. 2017. The coupled and uncoupled mechanisms by which trans-acting factors regulate mRNA stability and translation. J Biochem 161:309–314. https://doi.org/10.1093/jb/mvw086.
2. Kovarik P, Ebner F, Sedlyarov V. 2017. Posttranscriptional regulation of cytokine expression. Cytokine 89:21–26. https://doi.org/10.1016/j.cyto.2015.11.007.
3. Barreau C, Paillard L, Osborne HB. 2005. AU-rich elements and associated factors: are there unifying principles? Nucleic Acids Res 33:7138–7150. https://doi.org/10.1093/nar/gki1012.
4. Lai WS, Stumpo DJ, Blackshear PJ. 1990. Rapid insulin-stimulated accumulation of an mRNA encoding a proline-rich protein. J Biol Chem 265:16556–16563.
5. Cao H, Tuttle JS, Blackshear PJ. 2004. Immunological characterization of tristetraprolin as a low abundance, inducible, stable cytosolic protein. J Biol Chem 279:21489–21499. https://doi.org/10.1074/jbc.M400900200.
6. Stumpo DJ, Byrd NA, Phillips RS, Ghosh S, Maronpot RR, Castranio T, Meyers EN, Mishina Y, Blackshear PJ. 2004. Chorioallantoic fusion defects and embryonic lethality resulting from disruption of Zfp36L1, a gene encoding a CCCH tandem zinc finger protein of the tristetraprolin family. Mol Cell Biol 24:6445–6455. https://doi.org/10.1128/MCB.24.14.6445-6455.2004.
7. Stumpo DJ, Broxmeyer HE, Ward T, Cooper S, Hangoc G, Chung YJ, Shelley WC, Richfield EK, Ray MK, Yoder MC, Aplan PD, Blackshear PJ. 2009. Targeted disruption of Zfp36l2, encoding a CCCH tandem zinc finger RNA-binding protein, results in defective hematopoiesis. Blood 114:2401–2410. https://doi.org/10.1182/blood-2009-04-214619.
8. Stumpo DJ, Trempus CS, Tucker CJ, Huang W, Li L, Kluckman K, Bortner DM, Blackshear PJ. 2016. Deficiency of the placenta- and yolk sac-specific tristetraprolin family member ZFP36L3 identifies likely mRNA targets and an unexpected link to placental iron metabolism. Development 143:1424–1433. https://doi.org/10.1242/dev.130369.
9. Lai WS, Carballo E, Thorn JM, Kennington EA, Blackshear PJ. 2000. Interactions of CCCH zinc finger proteins with mRNA. Binding of tristetraprolin-related zinc finger proteins to Au-rich elements and destabilization of mRNA. J Biol Chem 275:17827–17837.
10. Blackshear PJ, Phillips RS, Ghosh S, Ramos SB, Richfield EK, Lai WS. 2005. Zfp36l3, a rodent X chromosome gene encoding a placenta-specific member of the tristetraprolin family of CCCH tandem zinc finger proteins. Biol Reprod 73:297–307. https://doi.org/10.1095/biolreprod.105.040527.
11. Taylor GA, Carballo E, Lee DM, Lai WS, Thompson MJ, Patel DD, Schenkman DI, Gilkeson GS, Broxmeyer HE, Haynes BF, Blackshear PJ. 1996. A pathogenetic role for TNF alpha in the syndrome of cachexia, arthritis, and autoimmunity resulting from tristetraprolin (TTP) deficiency. Immunity 4:445–454. https://doi.org/10.1016/S1074-7613(00)80411-2.

12. Carballo E, Lai WS, Blackshear PJ. 1998. Feedback inhibition of macrophage tumor necrosis factor-alpha production by tristetraprolin. Science 281:1001–1005. https://doi.org/10.1126/science.281.5379.1001.
13. Keffer J, Probert L, Cazlaris H, Georgopoulos S, Kaslaris E, Kioussis D, Kollias G. 1991. Transgenic mice expressing human tumour necrosis factor: a predictive genetic model of arthritis. EMBO J 10:4025–4031.
14. Ulich TR, Shin SS, del Castillo J. 1993. Haematologic effects of TNF. Res Immunol 144:347–354. https://doi.org/10.1016/S0923-2494(93)80079-E.
15. Carballo E, Blackshear PJ. 2001. Roles of tumor necrosis factor-alpha receptor subtypes in the pathogenesis of the tristetraprolin-deficiency syndrome. Blood 98:2389–2395. https://doi.org/10.1182/blood.V98.8.2389.
16. Lai WS, Carballo E, Strum JR, Kennington EA, Phillips RS, Blackshear PJ. 1999. Evidence that tristetraprolin binds to AU-rich elements and promotes the deadenylation and destabilization of tumor necrosis factor alpha mRNA. Mol Cell Biol 19:4311–4323. https://doi.org/10.1128/MCB.19.6.4311.
17. Carrick DM, Lai WS, Blackshear PJ. 2004. The tandem CCCH zinc finger protein tristetraprolin and its relevance to cytokine mRNA turnover and arthritis. Arthritis Res Ther 6:248–264. https://doi.org/10.1186/ar1441.
18. Brewer BY, Malicka J, Blackshear PJ, Wilson GM. 2004. RNA sequence elements required for high affinity binding by the zinc finger domain of tristetraprolin: conformational changes coupled to the bipartite nature of Au-rich MRNA-destabilizing motifs. J Biol Chem 279:27870–27877. https://doi.org/10.1074/jbc.M402551200.
19. Hudson BP, Martinez-Yamout MA, Dyson HJ, Wright PE. 2004. Recognition of the mRNA AU-rich element by the zinc finger domain of TIS11d. Nat Struct Mol Biol 11:257–264. https://doi.org/10.1038/nsmb738.
20. Lai WS, Kennington EA, Blackshear PJ. 2002. Interactions of CCCH zinc finger proteins with mRNA: non-binding tristetraprolin mutants exert an inhibitory effect on degradation of AU-rich element-containing mRNAs. J Biol Chem 277:9606–9613. https://doi.org/10.1074/jbc.M110395200.
21. Sandler H, Stoecklin G. 2008. Control of mRNA decay by phosphorylation of tristetraprolin. Biochem Soc Trans 36:491–496. https://doi.org/10.1042/BST0360491.
22. Brooks SA, Blackshear PJ. 2013. Tristetraprolin (TTP): interactions with mRNA and proteins, and current thoughts on mechanisms of action. Biochim Biophys Acta 1829:666–679. https://doi.org/10.1016/j.bbagrm.2013.02.003.
23. Kratochvill F, Machacek C, Vogl C, Ebner F, Sedlyarov V, Gruber AR, Hartweger H, Vielnascher R, Karaghiosoff M, Rulicke T, Muller M, Hofacker I, Lang R, Kovarik P. 2011. Tristetraprolin-driven regulatory circuit controls quality and timing of mRNA decay in inflammation. Mol Syst Biol 7:560. https://doi.org/10.1038/msb.2011.93.
24. Patial S, Blackshear PJ. 2016. Tristetraprolin as a therapeutic target in inflammatory disease. Trends Pharmacol Sci 37:811–821. https://doi.org/10.1016/j.tips.2016.07.002.
25. Tchen CR, Brook M, Saklatvala J, Clark AR. 2004. The stability of tristetraprolin mRNA is regulated by mitogen-activated protein kinase p38 and by tristetraprolin itself. J Biol Chem 279:32393–32400. https://doi.org/10.1074/jbc.M402059200.
26. Brooks SA, Connolly JE, Rigby WF. 2004. The role of mRNA turnover in the regulation of tristetraprolin expression: evidence for an extracellular signal-regulated kinase-specific, AU-rich element-dependent, autoregulatory pathway. J Immunol 172:7263–7271. https://doi.org/10.4049/jimmunol.172.12.7263.
27. Carballo E, Gilkeson GS, Blackshear PJ. 1997. Bone marrow transplantation reproduces the tristetraprolin-deficiency syndrome in recombination activating gene-2(−/−) mice. Evidence that monocyte/macrophage progenitors may be responsible for TNFalpha overproduction. J Clin Invest 100:986–995.
28. Qiu LQ, Stumpo DJ, Blackshear PJ. 2012. Myeloid-specific tristetraprolin deficiency in mice results in extreme lipopolysaccharide sensitivity in an otherwise minimal phenotype. J Immunol 188:5150–5159. https://doi.org/10.4049/jimmunol.1103700.
29. Qiu LQ, Lai WS, Bradbury A, Zeldin DC, Blackshear PJ. 2015. Tristetraprolin (TTP) coordinately regulates primary and secondary cellular responses to proinflammatory stimuli. J Leukoc Biol 97:723–736. https://doi.org/10.1189/jlb.3A0214-106R.
30. Kendall RT, Feghali-Bostwick CA. 2014. Fibroblasts in fibrosis: novel roles and mediators. Front Pharmacol 5:123. https://doi.org/10.3389/fphar.2014.00123.
31. Kalluri R. 2016. The biology and function of fibroblasts in cancer. Nat Rev Cancer 16:582–598. https://doi.org/10.1038/nrc.2016.73.
32. Lai WS, Parker JS, Grissom SF, Stumpo DJ, Blackshear PJ. 2006. Novel mRNA targets for tristetraprolin (TTP) identified by global analysis of stabilized transcripts in TTP-deficient fibroblasts. Mol Cell Biol 26:9196–9208. https://doi.org/10.1128/MCB.00945-06.
33. Ghosh S, Hoenerhoff MJ, Clayton N, Myers P, Stumpo DJ, Maronpot RR, Blackshear PJ. 2010. Left-sided cardiac valvulitis in tristetraprolin-deficient mice: the role of tumor necrosis factor alpha. Am J Pathol 176:1484–1493. https://doi.org/10.2353/ajpath.2010.090498.
34. Dinarello CA. 2009. Immunological and inflammatory functions of the interleukin-1 family. Annu Rev Immunol 27:519–550. https://doi.org/10.1146/annurev.immunol.021908.132612.
35. Dinarello CA, Simon A, van der Meer JW. 2012. Treating inflammation by blocking interleukin-1 in a broad spectrum of diseases. Nat Rev Drug Discov 11:633–652. https://doi.org/10.1038/nrd3800.
36. Carballo E, Lai WS, Blackshear PJ. 2000. Evidence that tristetraprolin is a physiological regulator of granulocyte-macrophage colony-stimulating factor messenger RNA deadenylation and stability. Blood 95:1891–1899.
37. Lai WS, Kennington EA, Blackshear PJ. 2003. Tristetraprolin and its family members can promote the cell-free deadenylation of AU-rich element-containing mRNAs by poly(A) ribonuclease. Mol Cell Biol 23:3798–3812. https://doi.org/10.1128/MCB.23.11.3798-3812.2003.
38. Blackshear PJ, Perera L. 2014. Phylogenetic distribution and evolution of the linked RNA-binding and NOT1-binding domains in the tristetraprolin family of tandem CCCH zinc finger proteins. J Interferon Cytokine Res 34:297–306. https://doi.org/10.1089/jir.2013.0150.
39. Wells ML, Perera L, Blackshear PJ. 2017. An ancient family of RNA-binding proteins: still important! Trends Biochem Sci https://doi.org/10.1016/j.tibs.2016.12.003.
40. Wells ML, Hicks SN, Perera L, Blackshear PJ. 2015. Functional equivalence of an evolutionarily conserved RNA binding module. J Biol Chem 290:24413–24423. https://doi.org/10.1074/jbc.M115.673012.
41. Zhu W, Brauchle MA, Di Padova F, Gram H, New L, Ono K, Downey JS, Han J. 2001. Gene suppression by tristetraprolin and release by the p38 pathway. Am J Physiol Lung Cell Mol Physiol 281:L499–L508.
42. Liang J, Lei T, Song Y, Yanes N, Qi Y, Fu M. 2009. RNA-destabilizing factor tristetraprolin negatively regulates NF-kappaB signaling. J Biol Chem 284:29383–29390. https://doi.org/10.1074/jbc.M109.024745.
43. Xu L, Ning H, Gu L, Wang Q, Lu W, Peng H, Cui W, Ying B, Ross CR, Wilson GM, Wei L, Wold WS, Liu J. 2015. Tristetraprolin induces cell cycle arrest in breast tumor cells through targeting AP-1/c-Jun and NF-kappaB pathway. Oncotarget 6:41679–41691. https://doi.org/10.18632/oncotarget.6149.
44. Phillips RS, Ramos SB, Blackshear PJ. 2002. Members of the tristetraprolin family of tandem CCCH zinc finger proteins exhibit CRM1-dependent nucleocytoplasmic shuttling. J Biol Chem 277:11606–11613. https://doi.org/10.1074/jbc.M111457200.
45. Pomeranz MC, Hah C, Lin PC, Kang SG, Finer JJ, Blackshear PJ, Jang JC. 2010. The Arabidopsis tandem zinc finger protein AtTZF1 traffics between the nucleus and cytoplasmic foci and binds both DNA and RNA. Plant Physiol 152:151–165. https://doi.org/10.1104/pp.109.145656.
46. Kim WC, Kim JY, Ko JH, Kang H, Kim J, Han KH. 2014. AtC3H14, a plant-specific tandem CCCH zinc-finger protein, binds to its target mRNAs in a sequence-specific manner and affects cell elongation in Arabidopsis thaliana. Plant J 80:772–784. https://doi.org/10.1111/tpj.12667.
47. Cao H, Deterding LJ, Blackshear PJ. 2007. Phosphorylation site analysis of the anti-inflammatory and mRNA-destabilizing protein tristetraprolin. Expert Rev Proteomics 4:711–726. https://doi.org/10.1586/14789450.4.6.711.
48. Carballo E, Cao H, Lai WS, Kennington EA, Campbell D, Blackshear PJ. 2001. Decreased sensitivity of tristetraprolin-deficient cells to p38 inhibitors suggests the involvement of tristetraprolin in the p38 signaling pathway. J Biol Chem 276:42580–42587. https://doi.org/10.1074/jbc.M104953200.
49. Zhang X, Chen X, Liu Q, Zhang S, Hu W. 2017. Translation repression via modulation of the cytoplasmic poly(A)-binding protein in the inflammatory response. Elife 6:e27786. https://doi.org/10.7554/eLife.27786.
50. Kedar VP, Darby MK, Williams JG, Blackshear PJ. 2010. Phosphorylation of human tristetraprolin in response to its interaction with the Cbl interacting protein CIN85. PLoS One 5:e9588. https://doi.org/10.1371/journal.pone.0009588.
51. Kedar VP, Zucconi BE, Wilson GM, Blackshear PJ. 2012. Direct binding of specific AUF1 isoforms to tandem zinc finger domains of tristetraprolin (TTP) family proteins. J Biol Chem 287:5459–5471. https://doi.org/10.1074/jbc.M111.312652.
52. Fabian MR, Frank F, Rouya C, Siddiqui N, Lai WS, Karetnikov A, Blackshear

PJ, Nagar B, Sonenberg N. 2013. Structural basis for the recruitment of the human CCR4-NOT deadenylase complex by tristetraprolin. Nat Struct Mol Biol 20:735–739. https://doi.org/10.1038/nsmb.2572.
53. Patial S, Curtis AD, II, Lai WS, Stumpo DJ, Hill GD, Flake GP, Mannie MD, Blackshear PJ. 2016. Enhanced stability of tristetraprolin mRNA protects mice against immune-mediated inflammatory pathologies. Proc Natl Acad Sci U S A 113:1865–1870. https://doi.org/10.1073/pnas.1519906113.
54. Redlich K, Smolen JS. 2012. Inflammatory bone loss: pathogenesis and therapeutic intervention. Nat Rev Drug Discov 11:234–250. https://doi.org/10.1038/nrd3669.
55. Jung SM, Kim KW, Yang CW, Park SH, Ju JH. 2014. Cytokine-mediated bone destruction in rheumatoid arthritis. J Immunol Res 2014:263625. https://doi.org/10.1155/2014/263625.
56. Kang JG, Amar MJ, Remaley AT, Kwon J, Blackshear PJ, Wang PY, Hwang PM. 2011. Zinc finger protein tristetraprolin interacts with CCL3 mRNA and regulates tissue inflammation. J Immunol 187:2696–2701. https://doi.org/10.4049/jimmunol.1101149.
57. Johnson RA, Wichern DW. 2002. Comparisons of several multivariate means, p 272–352. *In* Yagan S (ed), Applied multivariate statistical analysis, 5th ed. Prentice Hall, Upper Saddle River, NJ.
58. Laird NM, Ware JH. 1982. Random-effects models for longitudinal data. Biometrics 38:963–974. https://doi.org/10.2307/2529876.
59. Cremasco V, Decker CE, Stumpo D, Blackshear PJ, Nakayama KI, Nakayama K, Lupu TS, Graham DB, Novack DV, Faccio R. 2012. Protein kinase C-delta deficiency perturbs bone homeostasis by selective uncoupling of cathepsin K secretion and ruffled border formation in osteoclasts. J Bone Miner Res 27:2452–2463. https://doi.org/10.1002/jbmr.1701.
60. Zamani A, Decker C, Cremasco V, Hughes L, Novack DV, Faccio R. 2015. Diacylglycerol kinase zeta (DGKzeta) is a critical regulator of bone homeostasis via modulation of c-Fos levels in osteoclasts. J Bone Miner Res 30:1852–1863. https://doi.org/10.1002/jbmr.2533.
61. Lai WS, Perera L, Hicks SN, Blackshear PJ. 2014. Mutational and structural analysis of the tandem zinc finger domain of tristetraprolin. J Biol Chem 289:565–580. https://doi.org/10.1074/jbc.M113.466326.
62. Fortina P, Surrey S. 2008. Digital mRNA profiling. Nat Biotechnol 26:293–294. https://doi.org/10.1038/nbt0308-293.
63. Cao H. 2004. Expression, purification, and biochemical characterization of the antiinflammatory tristetraprolin: a zinc-dependent mRNA binding protein affected by posttranslational modifications. Biochemistry 43:13724–13738. https://doi.org/10.1021/bi049014y.